

# Most suitable evaluation method for adhesive strength to minimize bend effect in lap joints in terms of the intensity of singular stress field

著者	Rong Li, Noda Naoaki, Takaki Rei, Sano Yoshikazu, Takase Yasushi, Miyazaki Tatsujiro
journal or publication title	International Journal of Adhesion and Adhesives
volume	86
page range	45-58
year	2018-08-23
URL	<a href="http://hdl.handle.net/10228/00007859">http://hdl.handle.net/10228/00007859</a>

doi: <https://doi.org/10.1016/j.ijadhadh.2018.08.006>

## Author's Accepted Manuscript

Most suitable evaluation method for adhesive strength to minimize bend effect in lap joints in terms of the intensity of singular stress field

LI Rong, Nao-Aki Noda, Rei Takaki, Yoshikazu Sano, Yasushi Takase, Tatsujiro Miyazaki



PII: S0143-7496(18)30197-0  
DOI: <https://doi.org/10.1016/j.ijadhadh.2018.08.006>  
Reference: JAAD2252

To appear in: *International Journal of Adhesion and Adhesives*

Received date: 21 May 2018  
Accepted date: 9 August 2018

Cite this article as: LI Rong, Nao-Aki Noda, Rei Takaki, Yoshikazu Sano, Yasushi Takase and Tatsujiro Miyazaki, Most suitable evaluation method for adhesive strength to minimize bend effect in lap joints in terms of the intensity of singular stress field, *International Journal of Adhesion and Adhesives*, <https://doi.org/10.1016/j.ijadhadh.2018.08.006>

This is a PDF file of an unedited manuscript that has been accepted for publication. As a service to our customers we are providing this early version of the manuscript. The manuscript will undergo copyediting, typesetting, and review of the resulting galley proof before it is published in its final citable form. Please note that during the production process errors may be discovered which could affect the content, and all legal disclaimers that apply to the journal pertain.

# Most suitable evaluation method for adhesive strength to minimize bend effect in lap joints in terms of the intensity of singular stress field

Rong LI<sup>a,c</sup>, Nao-Aki NODA<sup>a,\*</sup>, Rei TAKAKI<sup>a</sup>, Yoshikazu SANO<sup>a</sup>, Yasushi TAKASE<sup>a</sup>, Tatsujiro MIYAZAKI<sup>b</sup>

<sup>a</sup>Department of Mechanical Engineering, Kyushu Institute of Technology, 1-1 Sensui-cho Tobata-ku, Kitakyushu-shi 804-8550, Japan

<sup>b</sup>Department of Mechanical Engineering, University of the Ryukyus, 1 Senbaru, Nishihara-cho, Nakagami-gun, Okinawa 903-0213, Japan

<sup>c</sup>School of Civil Engineering, Henan University of Science and Technology, Luoyang 471023, China

\*Corresponding author: Nao-Aki NODA, Department of Mechanical Engineering, Kyushu Institute of Technology, 1-1 Sensui-cho, Tobata-ku, Kitakyushu-shi, Fukuoka 804-8550, Japan, Tel: +81-080-3886-6069, E-mail: noda@mech.kyutech.ac.jp

## Abstract

The lap joint testing is designed to investigate the adhesive strength under pure shear loading. However, actually pure shear testing is very difficult to be realized in the experiment because of the bend deformation during testing causing the peeling force appearing at the adhesive region. To reduce the bend effect, this paper focuses on the intensity of singular stress field (ISSF) at the interface end in order to minimize the ISSF for lap joints. The results show that the ISSF decreases with increasing the adherend thickness. The minimum ISSF is obtained when the adherend thickness is large enough with the small deformation angle defined at the interface end. Since the strength of double lap joint (DLJ) is sometimes about two times larger than the strength of single lap joint

(SLJ), the equivalent strength condition is discussed by changing adherend thicknesses of DLJ and SLJ. It is found that the strength of SLJ with adherend thickness  $t_1=7\text{mm}$  is nearly equal to that of double lap joint with  $t_1=1.5\text{mm}$  prescribed in Japanese Industrial Standard.

## Keywords

Adhesion; Fracture mechanics; Intensity of singular stress field; Interfaces; single lap joint

## Nomenclature

$C_\sigma, C_\tau$  Constants defined as the ISSF ratio  $C_\sigma = K_{\sigma, \lambda_2} / K_{\sigma, \lambda_1}$ ,  $C_\tau = K_{\tau, \lambda_2} / K_{\tau, \lambda_1}$

$\ell$  Distance from center point of the loading surface to loading point

$E$  Young's modulus

$G$  Shear modulus

$L$  Fixed boundary length in Fig.3 (a), (b)

$K_\sigma$  ISSF, Intensity of singular stress field

$K_{\sigma c}$  Critical value of ISSF, critical intensity of singular stress field

$l_1$  Adherend length in Fig. 3 (a), (b)

$l_2$  Adherend length  $l_2 = l_1 - l_{ad} - d$  in Fig. 3 (a), (b)

$l_{ad}$  Bondline length in Fig. 3 (a), (b)

$P$  Load parameter  $P / W = \sigma_o t = 14.15\text{N/mm}$

$r$  Radial distance away from the corner point O in Fig.3 (a), (b)

$t_1$  Adherend thickness in Fig.3 (a), (b)

$t_{ad}$  Bondline thickness in Fig.3 (a), (b)

$t$  Adherend end thickness in Fig.3 (a), (b),  $t = 2t_1 + t_{ad}$

$\alpha, \beta$  Dundurs' material composite parameters defined in equation (2)

$\theta_{ol}, \theta_{or}$  Deformation angles at the interface corner O

$\theta_C$  Deformation angle at the interface corner C

$\lambda$  Singular index obtained from eigenequation (1)

$\sigma_y, \tau_{xy}$  Tension and shear stress component near the interface end (see Fig. 3)

$\sigma_0$  Tension stress at both ends of single lap joint

$\sigma_c$  Adhesive strength

$\tau_{ave}$  Average shear stress at fracture

$\nu$  Poisson's ratio

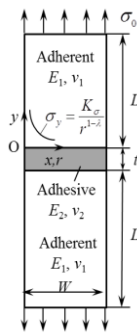
$W$  Joint width

## 1. Introduction

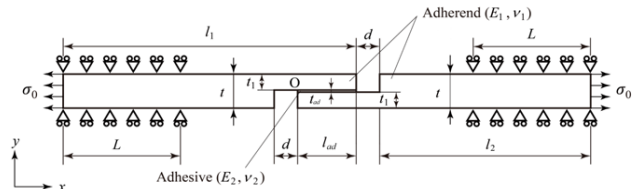
Due to the lower cost, high fatigue resistance and availability, structural adhesive has been widely used in a variety of industrial fields, such as automobile industry [1-4], shipbuilding [5,6], aircraft and spacecraft structures [7]. Structural adhesive has been replacing welding, screw, bolt, etc. It has been reported that the adhesive strength can be sometimes equivalent to the strength of the adherend [1, 2]. Recently, the authors have shown that the adhesive strength is controlled by the intensity of the singular stress field (ISSF) at the interface end. As shown in Fig. 1 (a) ~ (b), the butt joint strength can be expressed as a constant value of the critical ISSF  $K_{\sigma c} = \text{const.}$  [8]. Also, as shown in Fig. 1 (c) ~ (d) the lap joint strength can be expressed as  $K_{\sigma c} = \text{const.}$  [9-13]. Similarly, the adhesive bonded strength was previously expressed as  $H_{cr} = \text{const.}$  in [14, 15]. Since those previous studies indicated that the ISSF may control the adhesive strength [8-17], rational and practical ISSF methods can be used for evaluating the adhesive strength.

The testing method for the adhesive strength of lap joints is prescribed in Japanese Industrial Standards (JIS) [18]. However, usually the lap joint strength is affected by the specimen configuration. As an example, Fig. 2 (a) shows that the critical average shear stress of the double lap joint strength is nearly twice larger than the one of the single lap joint strength [19, 20]. Fig. 2 (b) shows that the critical average shear stress leading to the results in Fig. 1 (b) [21]. In Fig. 2 (b), among the specimens A20-15 ~ A50-15 having different bondline length  $l_{ad}$ , the critical average shear stress  $\tau_{ave}$  decreases with increasing the adhesive length. Therefore, Fig. 2 (b) shows the adhesive strength cannot be expressed as  $\tau_{ave} = \text{const.}$

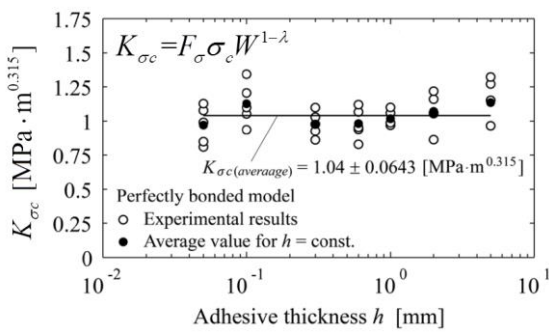
The single lap joint testing was originally intended to be conducted under pure shear loading, but actually the pure shear testing is very difficult to be realized experimentally. Due to the bend deformation during testing, the peeling force is always generated to prevent pure shear testing at the adhesive region. Since this peeling force is corresponding to the ISSF at the interface end, this study focuses on how to minimize the ISSF for single lap joint. Then, the effect of the specimen geometry on the ISSF will be discussed by considering the previous experimental studies [21]. Since the strength of double lap joint is usually much larger than the strength of single lap joint [19, 20], the equivalent conditions for the single and double lap joints will be also discussed in this paper.



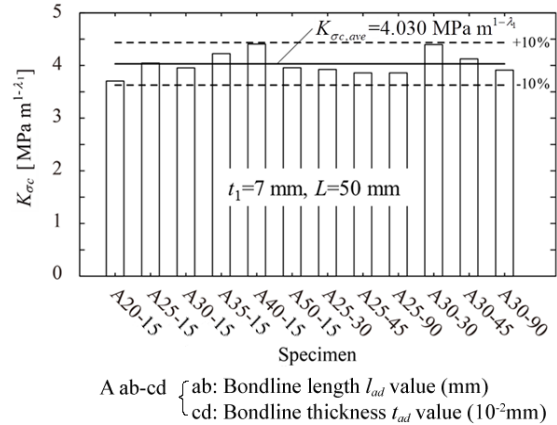
(a) Butt joint model [8]



(c) Single lap joint model [9-13]

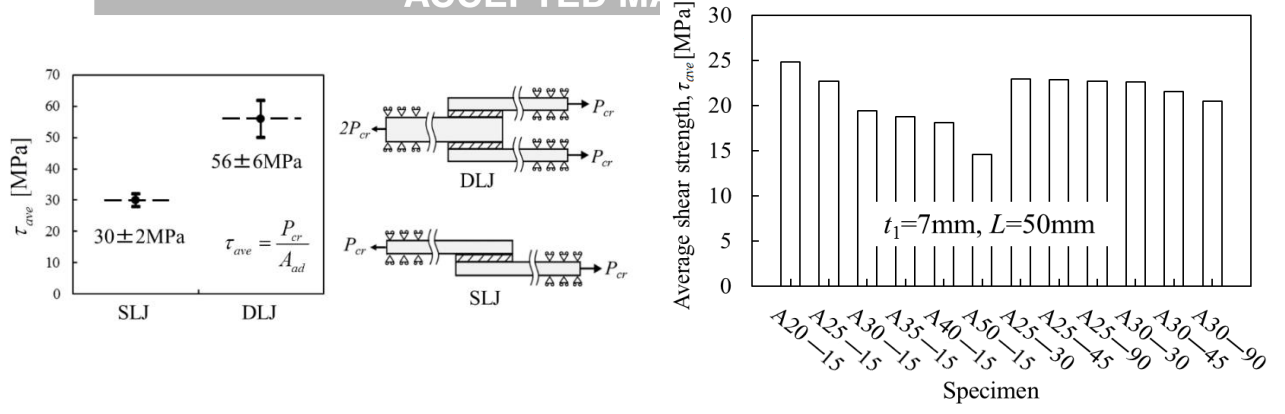


(b) Adhesive strength of butt joint [8]



(d) Adhesive strength of single lap joint [9-13]

Fig. 1 Adhesive strength expressed as a constant value of the critical ISSF  $K_{\sigma_c} = \text{const}$



(a) Critical average shear stress obtained by single lap joint (SLJ) and double lap joint (DLJ) when the adherend is S45C and the adhesive is epoxy [19, 20]

(b) Critical average shear stress experimentally obtained leading to the results in Fig.1(b) by varying bondline dimensions  $l_{ad}=20\text{-}50\text{mm}$  and  $t_{ad}=0.15\text{-}0.90\text{mm}$  when the adherend is aluminum alloy and the adhesive is epoxy [21]

Fig. 2. Adhesive strength expressed as an average shear stress

## 2. Lap joint modelling and mesh-independent technique to calculate the ISSF

In this section, the ISSF method to evaluate lap joint strength will be explained. The mesh-independent techniques to calculate the ISSF can be found in [9-13]. The singular stress field for lap joints is characterized by the singular index  $\lambda$ , which can be determined from eigenequation (1) [22-24]. As shown in Appendix A, Equation (1) has two real roots for most of the material combinations.

$$4 \sin^2(\pi\lambda) \left\{ \sin^2\left(\frac{\pi\lambda}{2}\right) - \lambda^2 \right\} \beta^2 + 4\lambda^2 \sin^2(\pi\lambda) \alpha\beta + \left\{ \sin^2\left(\frac{\pi\lambda}{2}\right) - \lambda^2 \right\} \alpha^2 - 4\lambda^2 \sin^2(\pi\lambda) \beta - 2 \left\{ \lambda^2 \cos(2\pi\lambda) + \sin^2\left(\frac{\pi\lambda}{2}\right) \cos(\pi\lambda) + \frac{1}{2} \sin^2(\pi\lambda) \right\} \alpha + \sin^2\left(\frac{3\pi}{2}\lambda\right) - \lambda^2 = 0 \quad (1)$$

Here,  $\alpha$  and  $\beta$  are Dundurs' parameters [25] defined by Poisson's ratio  $\nu$  and shear modulus  $G$  ( $m=1$  is for adhesive,  $m=2$  is for adherend).

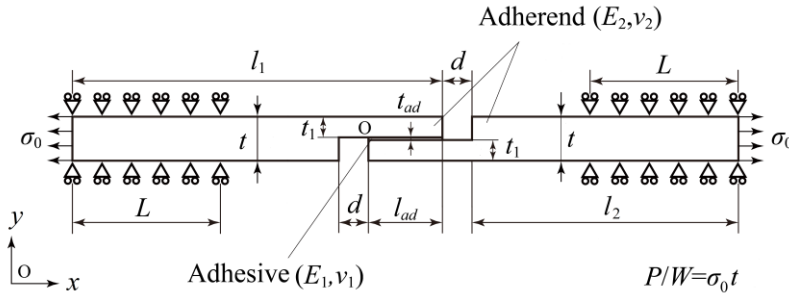
$$\alpha = \frac{G_1(\kappa_2 + 1) - G_2(\kappa_1 + 1)}{G_1(\kappa_2 + 1) + G_2(\kappa_1 + 1)}, \quad \beta = \frac{G_1(\kappa_2 - 1) - G_2(\kappa_1 - 1)}{G_1(\kappa_2 + 1) + G_2(\kappa_1 + 1)}, \quad \kappa_m = \begin{cases} \frac{3 - \nu_j}{1 + \nu_m} & \text{(plane stress)} \\ 3 - 4\nu_m & \text{(plane strain)} \end{cases} \quad (m = 1, 2). \quad (2)$$

Since the previous studies showed that the adhesive strength can be expressed as a constant value of the ISSF in 2D modelling [8-13], this study will discuss the effect of the specimen

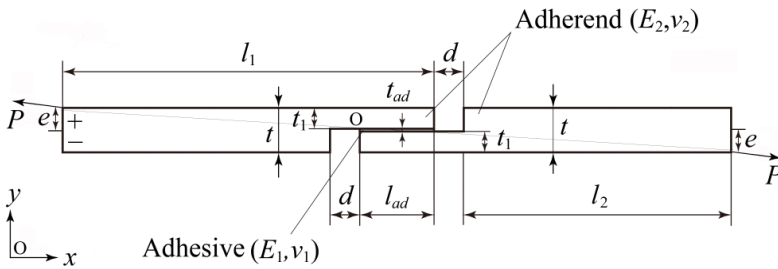
geometry on the ISSF. Table 1 shows the elastic parameters of the adherend and adhesive for the specimen used by Park et al [21]. Figure 3 shows two types of lap joint modelling by extending the specimen used in [21] with fixed bondline length  $l_{ad}=25\text{mm}$ , fixed bondline thickness  $t_{ad}=0.15\text{mm}$  under the load parameter  $P/W = \sigma_o t = 14.15\text{N/mm}$ . Here, the load parameter  $P/W = \sigma_o t = 14.15\text{N/mm}$  is corresponding to tensile stress  $\sigma_o = 1\text{MPa}$  in Park's specimen having the dimension  $t = 2t_1 + t_{ad} = (2 \times 7 + 0.15) = 14.15\text{mm}$  and  $W = 25\text{mm}$  [21]. The total length of the specimen in Fig.3 is  $225\text{mm}$  with  $d = 10\text{mm}$ . In Fig. 3 (a), the adherend thickness  $t_1$  and fixed boundary length  $L$  are mainly changed. In Fig. 3 (b), the tensile direction is mainly changed with the distance  $e$ .

**Table 1** Material properties of adherend and adhesive.

Materials	Young's modulus $\bar{E}$ [GPa]	Poisson's ratio $\nu$	$\alpha$	$\beta$	$\lambda_1$	$\lambda_2$
Adherend Aluminum alloy 6061- T6	68.9	0.3	-0.8699	-0.06642	0.6062	0.9989
Adhesive Epoxy resin	4.2	0.45				



(a) Lap joint model where the adherend thickness  $t_1$  and fixed boundary length  $L$  are mainly changed with fixed dimensions  $l_{ad} = 25\text{mm}$  and  $t_{ad} = 0.15\text{mm}$  under  $P/W = \sigma_o t = 14.15\text{N/mm}$



(b) Lap joint model where the tensile direction is mainly changed with fixed dimensions  $l_{ad} = 25\text{mm}$  and  $t_{ad} = 0.15\text{mm}$  under  $P/W = 14.15\text{N/mm}$



Fig. 3 Analysis model and boundary condition

The stresses  $\sigma_y$  and  $\tau_{xy}$  around the interface end can be expressed as follows. The notation  $r$  denotes the radial distance away from the corner singular point O.

$$\sigma_y = \frac{K_{\sigma,\lambda_1}}{r^{1-\lambda_1}} + \frac{K_{\sigma,\lambda_2}}{r^{1-\lambda_2}} \cong \frac{K_{\sigma,\lambda_1}}{r^{1-\lambda_1}} (1 + C_\sigma r^{\lambda_2-\lambda_1}), \tau_{xy} = \frac{K_{\tau,\lambda_1}}{r^{1-\lambda_1}} + \frac{K_{\tau,\lambda_2}}{r^{1-\lambda_2}} \cong \frac{K_{\tau,\lambda_1}}{r^{1-\lambda_1}} (1 + C_\tau r^{\lambda_2-\lambda_1}). \quad (3)$$

$$C_\sigma = K_{\sigma,\lambda_2}/K_{\sigma,\lambda_1}, \quad C_\tau = K_{\tau,\lambda_2}/K_{\tau,\lambda_1}.$$

Here,  $K_{\sigma,\lambda_1}$  and  $K_{\sigma,\lambda_2}$  denote the ISSFs. The previous studies showed that the ratios  $C_\sigma = K_{\sigma,\lambda_2}/K_{\sigma,\lambda_1}$  and  $C_\tau = K_{\tau,\lambda_2}/K_{\tau,\lambda_1}$  are almost constants except for extreme adhesive geometry [8-13]. The effects of  $K_{\sigma,\lambda_2}/r^{1-\lambda_2}$  and  $K_{\tau,\lambda_2}/r^{1-\lambda_2}$  in Eq. (3) may be very small since  $\lambda_2 \approx 1$ . Also it is known that  $K_{\sigma,\lambda_1}$  and  $K_{\tau,\lambda_1}$  are expressed by a single ISSF parameter [9-13], and therefore, both ISSFs in Eq. (3) can be controlled by  $K_{\sigma,\lambda_1}$  alone.

In this study, the reference solution is denoted by  $K_{\sigma,\lambda_1}^*$  and the unknown solution is denoted by  $K_{\sigma,\lambda_1}$ . Then, FEM stresses obtained by the finite element method (FEM) are denoted by  $\sigma_{y0,FEM}^*$  for the reference solution and  $\sigma_{y0,FEM}$  for unknown problem. Thus, from Eq. (3), the relation between  $K_{\sigma,\lambda_1}/K_{\sigma,\lambda_1}^*$  and  $\sigma_{y0,FEM}/\sigma_{y0,FEM}^*$  can be expressed as follows.

$$\frac{K_{\sigma,\lambda_1}}{K_{\sigma,\lambda_1}^*} = \frac{\sigma_{y0,FEM}}{\sigma_{y0,FEM}^*} \quad (4)$$

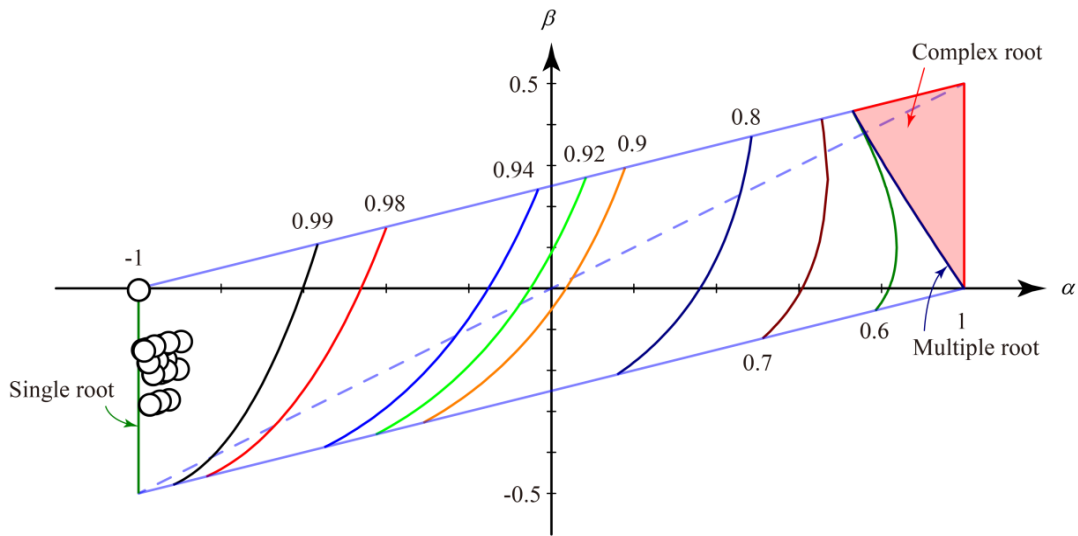
If the reference ISSF  $K_{\sigma,\lambda_1}^*$  is available,  $K_{\sigma,\lambda_1}$  can be obtained from the FEM stress ratio by applying the same mesh pattern to the reference problem [8-13]. In Eq.(4), the reference solution  $K_{\sigma,\lambda_1}^*$  can be obtained by using the Reciprocal Work Contour Integral Method (RWCIM). The detail information of the calculation process and the exact value of the reference solution  $K_{\sigma,\lambda_1}^*$  were presented in [13]. Then,  $K_{\sigma,\lambda_1}$  can be obtained from the FEM stress ratio by applying the same mesh pattern to the reference problem.

Table 2 shows the singular indexes  $\lambda_1, \lambda_2$  for several material combinations considered in [26, 27] including stainless steel SUS304, aluminum alloy A7075, silicon and IC substrate FR-4.5 as the adherends with resin as the adhesive. It is found that the weaker singular index  $\lambda_2=0.9914\sim 0.9999\approx 1$ , which is close to no singularity as  $\lambda_2=1$ .

**Table 2** Singular indexes for single lap joint with different material combinations.

	Material	Young's modulus $E$ [GPa]	Poisson's ratio $\nu$	$\lambda_1$	$\lambda_2$
Adherend	SUS304(stainless steel)	206	0.3	0.6568	0.9999
	A7075(aluminum alloys)	71	0.33	0.6489	0.9995
	Silicon	166	0.26	0.6552	0.9999
	FR-4.5(IC substrate)	15.34	0.15	0.6020	0.9914
Adhesive	Resin	2.74	0.38		

Figure 4 shows  $\lambda_2$  values on  $(\alpha, \beta)$  map for all material combinations. In Fig. 4, open circles ( $\circ$ ) denote the results for several metals-resin combinations. All metal-resin combinations are in the range  $E_1 = 108.4 - 206$  GPa,  $\nu_1 = 0.249 - 0.300$ ,  $E_2 = 0.037 - 3.6$  GPa,  $\nu_2 = 0.294 - 0.498$ . Then, it is seen that all open circle marks are in the range  $\lambda_2 = 0.99-1$ . Since always  $\lambda_2 \approx 1$ , the present method may be useful for evaluating all metal-resin lap joints.



$\circ$   $\lambda_2$  for the material combinations of metals ( $E_2 = 108.4 \sim 206$  GPa,  $\nu_2 = 0.249 \sim 0.300$ ) and adhesives ( $E_1 = 0.037 \sim 3.6$  GPa,  $\nu_1 = 0.294 \sim 0.498$ ) which are generally used in adhesive joints

Fig.4 Values of singular index  $\lambda_2$  on  $(\alpha, \beta)$  map.

Fig. 5 shows an example of FEM mesh around the interface end. The linear elastic analyses are performed under the plane strain condition by using the software MSC Marc. The element types chosen are quad 4 and quad 8. Here, 8-node elements are used in the vicinity of the interface end,

4-node elements are used in other regions. The minimize element size around the corner  $e_{\min}$  is  $3^{-12}$ mm. Note that the mesh-independent technique used in this study 4-node element is enough and 8-node element is not necessary since the FEM error can be eliminated by using the FEM ratio. However, 8-node elements are more convenient to obtain the reference solution by calculating the path integrals in RWCIM [9-13].

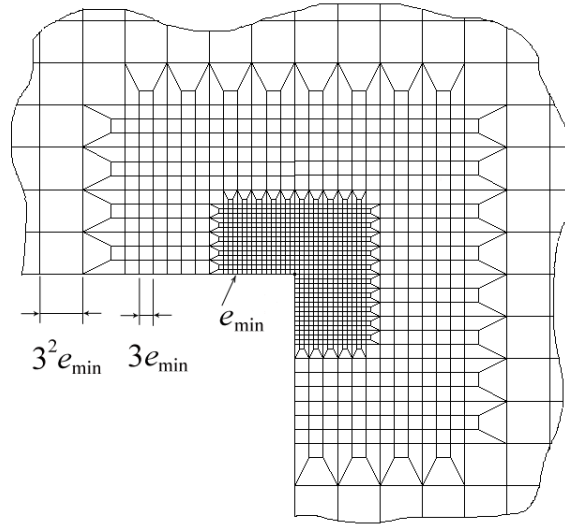


Fig. 5 Mesh pattern around the interface end.

As shown in Fig.6, the bend deformation can be described by focusing on the deformation angle  $\theta_C$  at the interface end C. The detail information for the deformation angle  $\theta_C$  is indicated in Appendix B. In this study, the deformation angle  $\theta_C$  at the interface end C is determined from Point C and Point D with distance  $l_\theta$ . Table 3 shows the effect of  $l_\theta$  on  $\theta_C$  by varying the minimum mesh size  $e_{\min}$  by taking an example of  $t_1=7$ mm,  $L=50$ mm and  $l_2=90$ mm. Due to the singular stress field around the interface end, the  $\theta_C$  value varies depending on  $l_\theta$ . In Table 3 it is seen that  $\theta_C$  is insensitive to minimum mesh size  $e_{\min}$ . Therefore, in this study, the maximum value of  $\theta_C$  is used to discuss the bend deformation. The  $l_\theta$  value giving the maximum  $\theta_C$  is depending on the interface end shape and material combination. In Table 3, the maximum value of  $\theta_C$  appears at  $l_\theta = 1/3^3$  independent of the minimum mesh size  $e_{\min}$ . The reason why  $\theta_C$  has a peak value near  $l_\theta=0$  is explained in Appendix B.

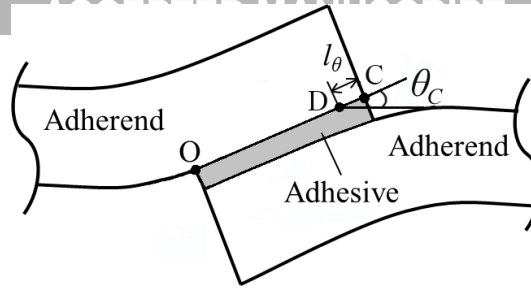


Fig.6 Deformation near the interface end.

**Table 3** Deformation angle  $\theta_C$  with varying  $e_{\min}$  and  $l_\theta$

$l_\theta$ [mm]	$\theta_C$		
	$e_{\min}=1/3^{11}$ mm	$e_{\min}=1/3^8$ mm	$e_{\min}=1/3^5$ mm
$1/3^4$	0.0186	0.0188	0.0187
$1/3^3$	0.0194	0.0194	0.0194
$1/3^2$	0.0188	0.0188	0.0188
$1/3$	0.0162	0.0162	0.0162

In lap joint specimens experimentally used, adhesive fillets may exist at the bonded ends as shown in Fig.7 (a). In this study, the local geometry as shown in Fig.5 has been assumed. If the local geometry is changed by the fillet, the singular stress field and the singular index are changed. Then, the adhesive strength evaluation becomes difficult. FEM analysis has shown that the stress concentration may decrease at the interface end by introducing the fillets [28]. However, Arai and Kobayashi [29] have shown that the debonding of the fillet occurs when the load is smaller than the final fracture. They have concluded that the specimens with and without fillet in Fig.7 (a), (b) have nearly the same strength. Similarly, Campilho, Moura and Domingues have analyzed the effect of the fillet geometries on the strength [30]. They have reported that the modelling validity is confirmed experimentally and the strength in Fig.7(a) is just slightly larger than the strength in Fig.7(b). Since those previous studies show that the fillet effect in Fig. 7 (a) is not very large, the authors think that the ISSF modelling as shown in Fig.7 (b) can be applied to other adhesive geometries including fillet. This might be analogous to continuing use of the SIFs (Stress Intensity Factors) in crack problems even though the small scale yielding is violated.

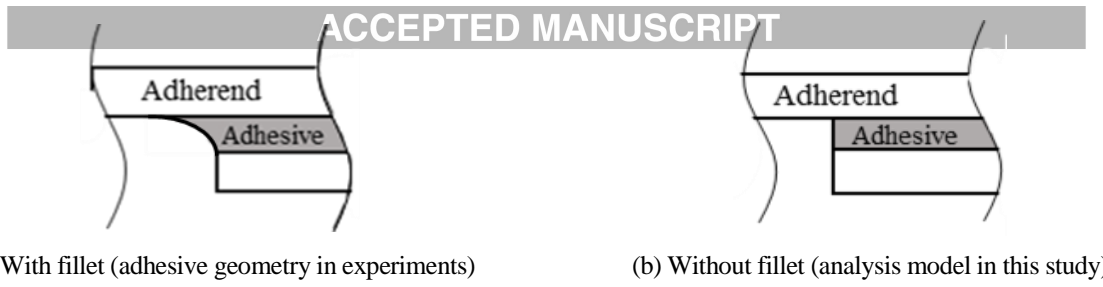


Fig. 7 Fillet at bonded edge

### 3. Pure shear testing to minimize ISSF and bend effect

In this section, the most suitable lap joint testing is investigated to minimize bend effect in terms of the ISSF under the same magnitude of load  $P/W = 14.15 \text{ N/mm}$  ( $\sigma_o = 1 \text{ MP}$  when  $t = 14.15 \text{ mm}$ ). In simulation process, the fixed boundary length  $L$  and the adherend thickness  $t_1$  in Fig.3 (a) and loading direction in Fig.3 (b) will be changed under fixed  $l_{ad} = 25 \text{ mm}$  and  $t_{ad} = 0.15 \text{ mm}$ . The effects of bondline length  $l_{ad}$  and bondline thickness  $t_{ad}$  were studied previously [9-13] (see Appendix C). The material combination is also fixed as shown in Table 1 since the ISSF should be compared under the same singular index  $\lambda_1$  and  $\lambda_2$ .

First, a special case is considered as shown in Fig. 8 to obtain the minimum value of ISSF  $K_{\sigma, \lambda_1} = K_{\sigma, \min}$ . In Fig.8 (a),  $t_1$  is changed when the adherends are fixed along the whole boundary ( $L = l_1$  or  $l_2$  in Fig.3 (a)) for the fixed dimensions of  $l_{ad} = 25 \text{ mm}$  and  $t_{ad} = 0.15 \text{ mm}$  under the load  $P/W = \sigma_o t = 14.15 \text{ N/mm}$ . Note that appropriate dimensionless expression for Fig.8 is difficult since the lap joint in Fig.3 has a complicated form. For butt joint specimen in Fig.1 (a), the dimensionless factors to control the ISSF have been clarified in the recent study [31]. In Fig. 8, with increasing adherend thickness  $t_1$ , the  $K_{\sigma, \lambda_1}$  decreases initially and then slightly increases, and finally becomes almost constant when  $t_1$  is large enough. The minimum ISSF  $K_{\sigma, \min} = 0.0422 \text{ MPa} \cdot \text{m}^{1-\lambda_1}$  can be obtained when  $t_1 = 13 \text{ mm}$ .

Fig. 8 (b) shows the minimum deformation angle  $\theta_C = \theta_{C, \min}$ . With increasing the adherend thickness  $t_1$ , the deformation angle  $\theta_C$  first decreases, then increases slightly and finally becomes constant when  $t_1$  is large enough. The minimum angle  $\theta_{C, \min} = 0.0042$  degree can be obtained when  $t_1 = 13 \text{ mm}$ .

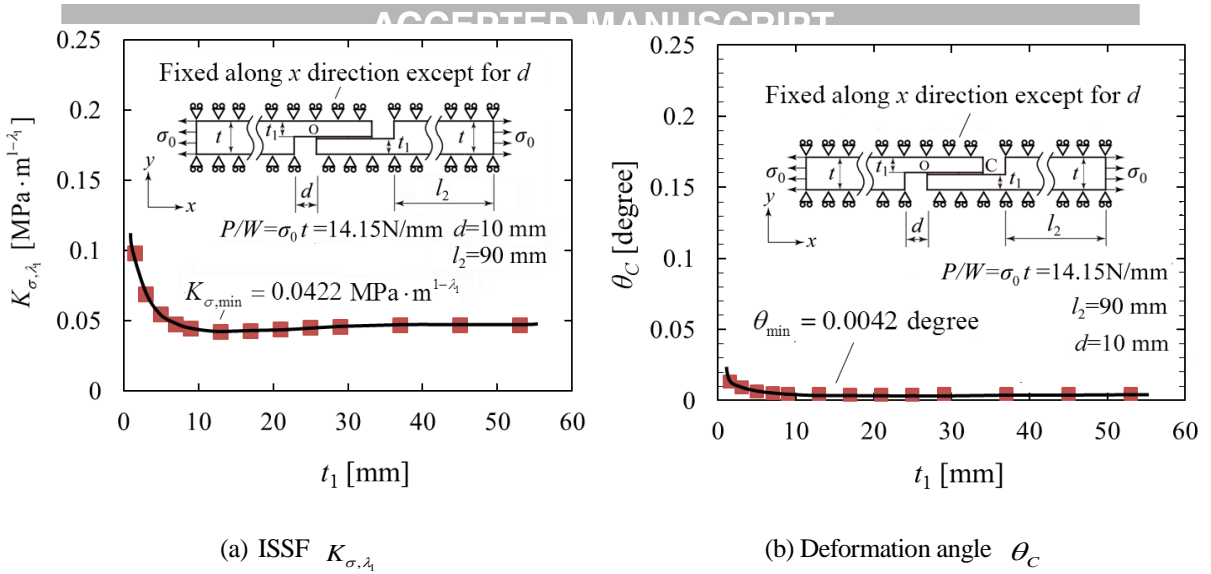


Fig. 8 Effect of adherend thickness  $t_1$  when  $L =$  the whole boundaries ( $=l_1$  or  $l_2$ ) for fixed dimensions  $l_{ad} = 25\text{mm}$  and  $t_{ad} = 0.15\text{mm}$  in Fig.3 (a) under  $P/W = \sigma_0 t = 14.15\text{N/mm}$

Fig. 9 (a) shows the results for fixed boundary length  $L = 50\text{mm}, 80\text{mm}, 90\text{mm}$ . Here, the notation JIS\* denotes the results of JIS K6850 prescribing the adherend thickness  $t_1 = 1.5\text{mm}$  and  $L = 50\text{mm}$ . The dashed line shows the minimum ISSF value  $K_{\sigma, \min} = 0.0422 \text{MPa} \cdot \text{m}^{1-\lambda_1}$ . With increasing  $t_1$ , the ISSF  $K_{\sigma, \lambda_1}$  decreases and becomes constant when  $t_1$  is large enough. When  $t_1 \geq 25\text{mm}$ , the effect of  $L$  can be ignored. The value  $K_{\sigma, \lambda_1} |_{t_1=1.5\text{mm}} = 0.2270 \text{MPa} \cdot \text{m}^{1-\lambda_1}$  of JIS K6850 is 5 times larger than the value of  $K_{\sigma, \min}$ . The value of Park's specimen [21]  $K_{\sigma, \lambda_1} |_{t_1=7\text{mm}} = 0.1010 \text{MPa} \cdot \text{m}^{1-\lambda_1}$  is still more than twice larger than  $K_{\sigma, \min} = 0.0422 \text{MPa} \cdot \text{m}^{1-\lambda_1}$ . The results show that the specimen [21] is much better than the JIS to obtain the adhesive strength, but still insufficient to obtain  $K_{\sigma, \min} = 0.0422 \text{MPa} \cdot \text{m}^{1-\lambda_1}$ . An international standard ASTM D5656 specifies the adhesive adherend thickness  $9.53\text{mm}$  for pure shear strength characterization. Fig. 9 shows that adherend thickness  $t_1 = 9.53\text{mm}$  is much better than the one of JIS specimens, but still insufficient to obtain the minimum ISSF.

Fig.9 (b) shows the results of deformation angle  $\theta_C$  when  $L = 50\text{mm}$  since in most of the previous experiments  $L \cong 50\text{mm}$ . Fig.9 (b) shows  $\theta_C$  decreases rapidly and then become constant with increasing  $t_1$ . The minimum  $\theta_C$  expressed as the dashed line can be obtained when  $t_1$  is large enough. The value  $\theta_C |_{t_1=1.5\text{mm}} = 0.1834$  degree of JIS specimen is about 40

times larger than the minimum angle  $\theta_{C,\min}$ . The value  $\theta_C|_{t_1=7\text{mm}}=0.0193$  degree of Park [21] is about 4 times larger than that the minimum angle  $\theta_{C,\min}$ . It is seen that the specimen in [21] is much better than the JIS, but insufficient to obtain the minimum value  $\theta_{C,\min}=0.0042$  degree.

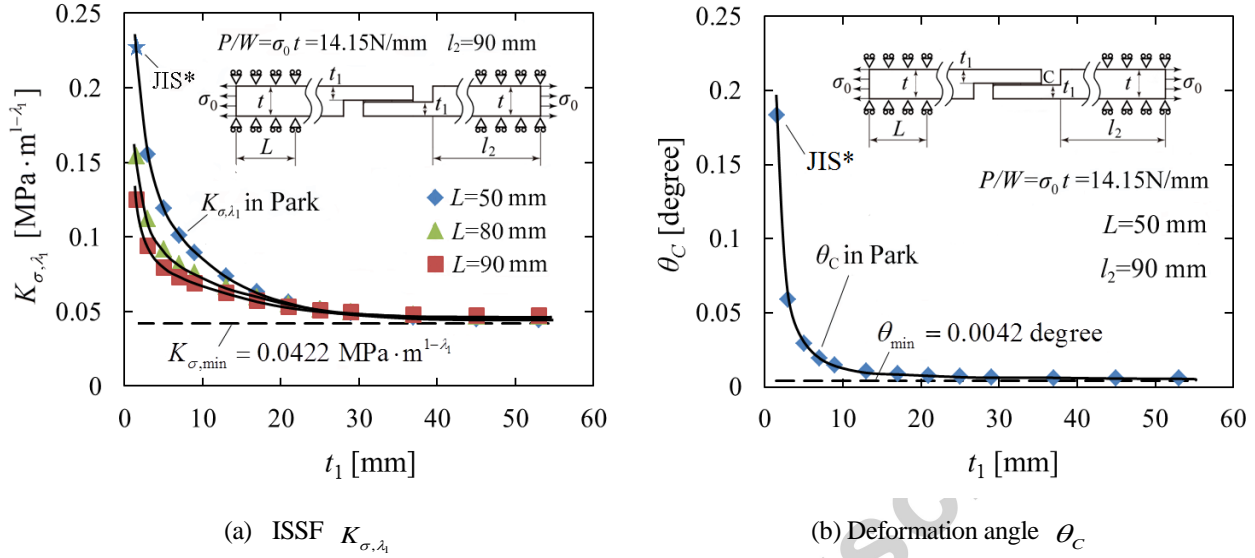


Fig.9 Effects of adherend thickness  $t_1$  when  $L = 50, 80, 90$ mm for fixed dimensions  $l_{ad}=25$ mm and  $t_{ad}=0.15$ mm in Fi.3 (a) under  $P/W = \sigma_0 t = 14.15$ N/mm (JIS\*: JIS K6850 prescribes specimen when  $t_1=1.5$ mm,  $L=50$ mm)

Fig. 10 (a) shows the effect of adherend length  $l_2$  on the ISSF  $K_{\sigma,\lambda_1}$  when  $t_1=7$ mm and  $L=50$ mm in Fig.3 (a). Only in Fig.10, the total specimen length is changed as 145~335mm by changing  $l_2$  but in other Figures the total length is always fixed as 225mm. The dashed line shows the minimum value  $K_{\sigma,\min} = 0.0422 \text{ MPa} \cdot \text{m}^{1-\lambda_1}$  when  $t_1=53$ mm. When  $t_1=7$ mm, with increasing adherend length  $l_2$ , the ISSF  $K_{\sigma,\lambda_1}$  increases. However, when  $t_1=53$ mm, the  $K_{\sigma,\lambda_1}$  is almost constant. In other words, the effect of adherend length  $l_2$  can be ignored when  $t_1$  is large enough. This is because the large adherend thickness may eliminate bending effect since the adherend becomes rigid enough. It may be concluded that  $K_{\sigma,\lambda_1}$  can be minimized by using small  $l_2$  and large  $t_1$ .

Fig. 10 (b) shows the results of deformation angle  $\theta_C$  when  $t_1=7$ mm. The dashed line shows the minimum value  $\theta_{C,\min}=0.0042$ degree when  $t_1=53$ mm. With increasing  $l_2$ ,  $\theta_C$  increases for  $t_1=7$ mm, but  $\theta_C$  is almost constant for  $t_1=53$ mm. When  $t_1$  is large enough, the minimum  $\theta_{C,\min}$

=0.0042 degree can be obtained easily since the effect of  $l_2$  on  $\theta_C$  can be ignored.

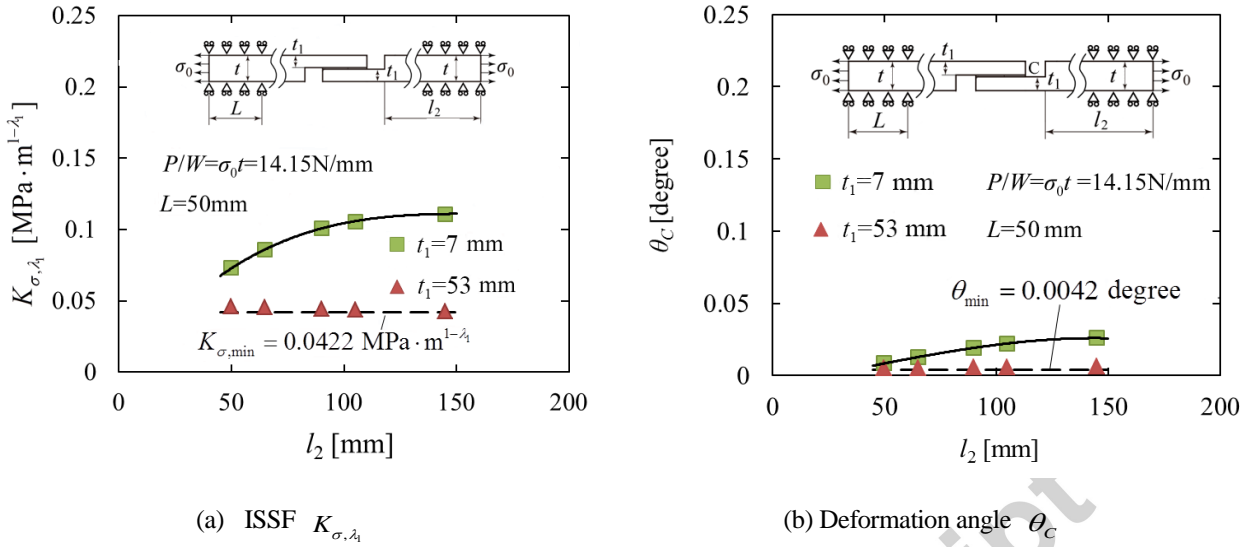


Fig. 10 Effects of adherend length  $l_2$  on  $K_{\sigma, \lambda_1}$  when  $t_1 = 7, 53 \text{ mm}$  and  $L = 50 \text{ mm}$  in Fig.3 (a) under fixed  $l_{ad} = 25 \text{ mm}$ ,  $t_{ad} = 0.15 \text{ mm}$  and  $P/W = \sigma_0 t = 14.15 \text{ N/mm}$  (In Fig.10, the total length of the specimen is changed as 145~335mm, in other Figures the total length is always fixed as 225mm)

As mentioned in Section 2, the previous study showed  $C_\sigma$  and  $C_\tau$  in Eq. (3) are almost constant independent of adhesive geometry. In a similar way, Fig.11 shows the effect of adherend geometry on  $C_\sigma$  and  $C_\tau$ . In Fig. 11,  $C_\sigma$  and  $C_\tau$  values are indicated by varying  $l_{ad} = 10 \sim 50 \text{ mm}$ ,  $t_{ad} = 0.15 \sim 0.9 \text{ mm}$ ,  $t_1 = 5 \sim 53 \text{ mm}$ ,  $l_2 = 50 \sim 145 \text{ mm}$ ,  $L = 50 \sim 90 \text{ mm}$  in Fig.3 (a). From Fig.11, we have  $C_\sigma = -5.0595 \pm 0.5467$ ,  $C_\tau = 0.2304 \pm 0.0249$ . The variations of  $C_\sigma$  and  $C_\tau$  are small except for the cases of small adherend thickness. For example, for small adherend thickness  $t_1 = 1.5$  and  $t_1 = 3 \text{ mm}$ , we have  $C_\sigma|_{t_1=1.5 \text{ mm}} = -9.8942$ ,  $C_\sigma|_{t_1=3 \text{ mm}} = -7.4799$ ,  $C_\tau|_{t_1=1.5 \text{ mm}} = 0.4505$ ,  $C_\tau|_{t_1=3 \text{ mm}} = 0.3406$  even other geometries are the same as  $l_{ad} = 25 \text{ mm}$ ,  $t_{ad} = 0.15 \text{ mm}$ ,  $l_2 = 90 \text{ mm}$ ,  $L = 50 \text{ mm}$ . This large discrepancy between small and large thickness specimens can be explained from the difference of the bend deformation.



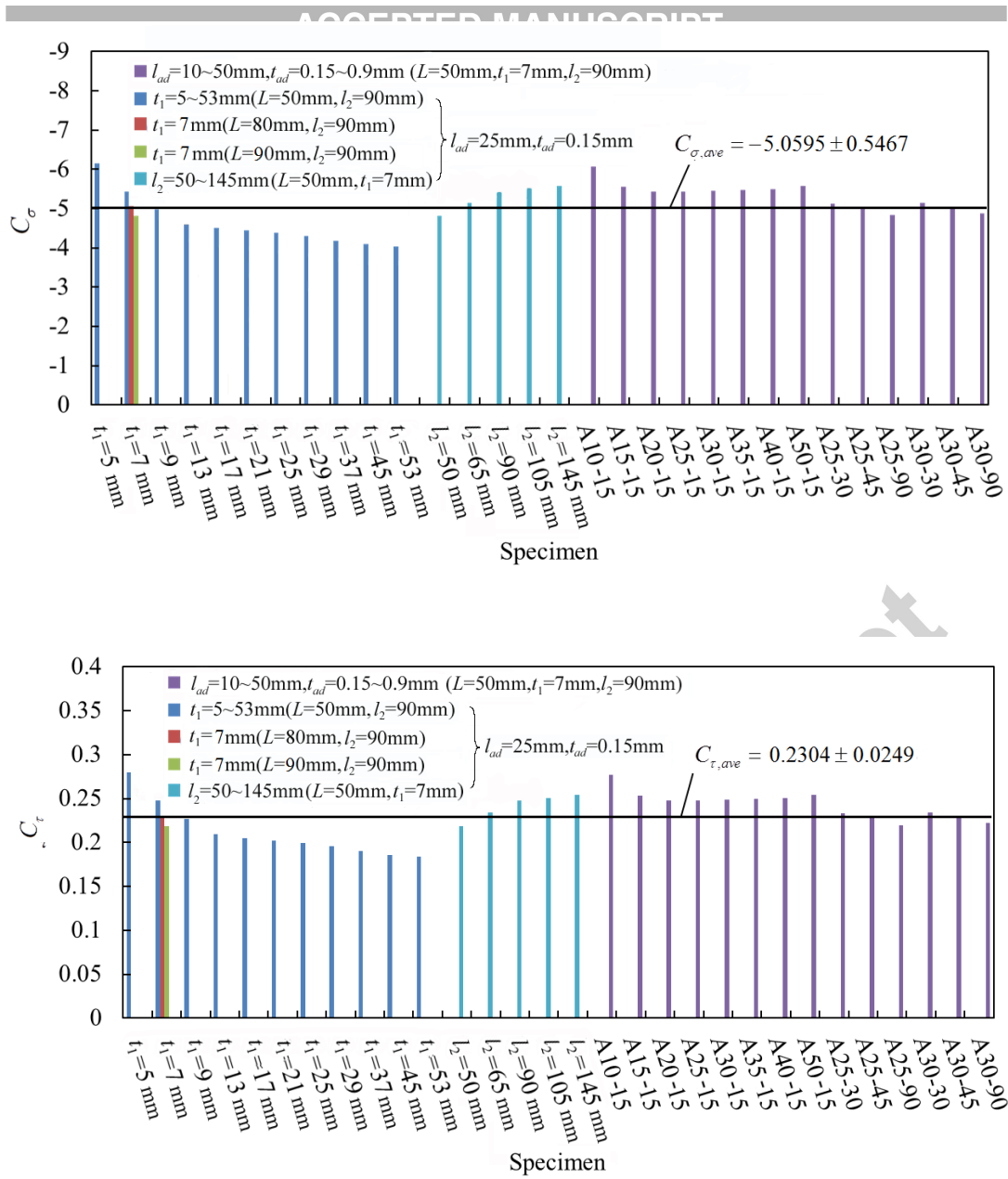


Fig. 11 (a) Results of  $C_\sigma$  for single lap joint with different specimen geometries, (b) Results of  $C_\tau$  for single lap joint with different specimen geometries

Fig. 12 (a) shows the relationship between the ISSF  $K_{\sigma,\lambda_1}$  and the eccentric distance  $\ell$  in Fig. 3(b). It is found that the  $K_{\sigma,\lambda_1}$  decreases with increasing the positive distance  $\ell$ . The effect of  $\ell$  on  $K_{\sigma,\lambda_1}$  becomes larger when the adherend thickness is smaller as  $t_1=7\text{mm}$ . When  $t_1=25\text{mm}$ ,  $K_{\sigma,\lambda_1}$  is almost constant independent of  $\ell$ .

Fig.12 (b) shows the relationship between deformation angle  $\theta_C$  and eccentric distance  $\ell$  in Fig.3 (b). It is found that  $\theta_C$  decreases with increasing  $\ell$ . The effect of  $\ell$  on  $\theta_C$  is significant when the adherend thickness is small when  $t_1=7\text{mm}$ . When  $t_1=25\text{mm}$ ,  $\theta_C$  is almost constant

independent of  $e$ .

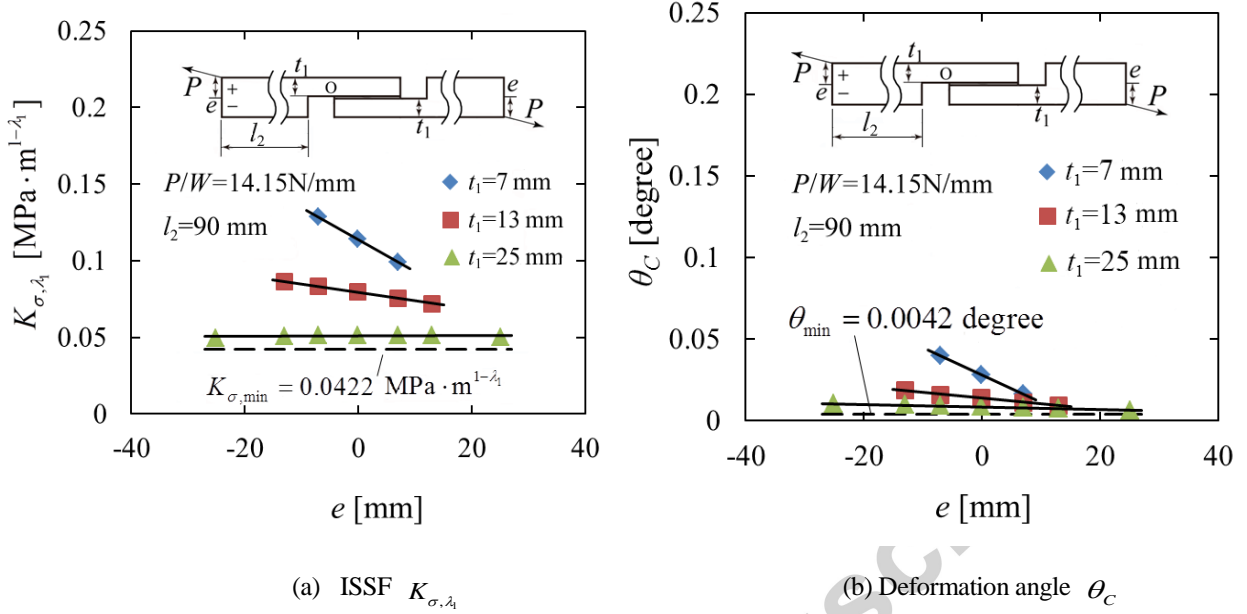


Fig.12 Effects of distance  $e$  when and adherend thickness  $t_1=7, 13, 25$  mm in Fig.3 (b) under fixed  $l_{ad}=25$ mm,  $t_{ad}=0.15$ mm and  $P/W=14.15$ N/mm

#### 4. Relationship between ISSF and deformation angle at the interface corner

As shown in Fig.8~Fig.10 and Fig.12, similar variations can be seen for ISSF  $K_{\sigma, \lambda_1}$  and deformation angle  $\theta_C$ . Fig. 13 shows the relation between  $K_{\sigma, \lambda_1}$  and  $\theta_C$  by using all results discussed in Section 3. As can be seen from Fig.13,  $K_{\sigma, \lambda_1}$  is controlled by  $\theta_C$  uniquely and  $K_{\sigma, \lambda_1}$  decreases with decreasing  $\theta_C$ . In other words,  $K_{\sigma, \lambda_1}$  variation can be explained by  $\theta_C$  and similarly  $\theta_C$  variation can be explained by  $K_{\sigma, \lambda_1}$ . As an example, when adherend thickness  $t_1=1.5$ mm prescribed by JIS, both  $K_{\sigma, \lambda_1}$  and  $\theta_C$  are very large. The minimum  $K_{\sigma, \lambda_1}$  and  $\theta_C$  can be obtained when the adherend thickness  $t_1$  is large enough as  $t_1 \geq 25$ mm. It is seen that the bend effect is minimized when  $t_1 \geq 25$ mm. The reason why the minimum  $K_{\sigma, \lambda_1} \neq 0$  can be explained by  $\theta_C \neq 0$  due to the local bend deformation at the interface end, which can be observed even for very large thickness. Therefore, the bend effect in single lap joint can be minimized when the adherend

thickness is large enough.

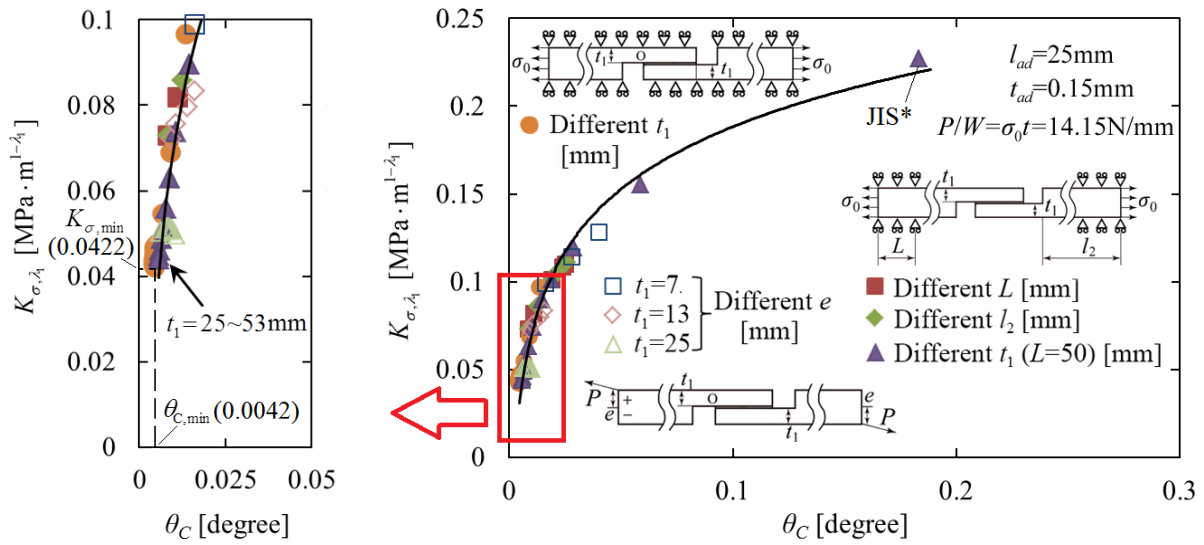
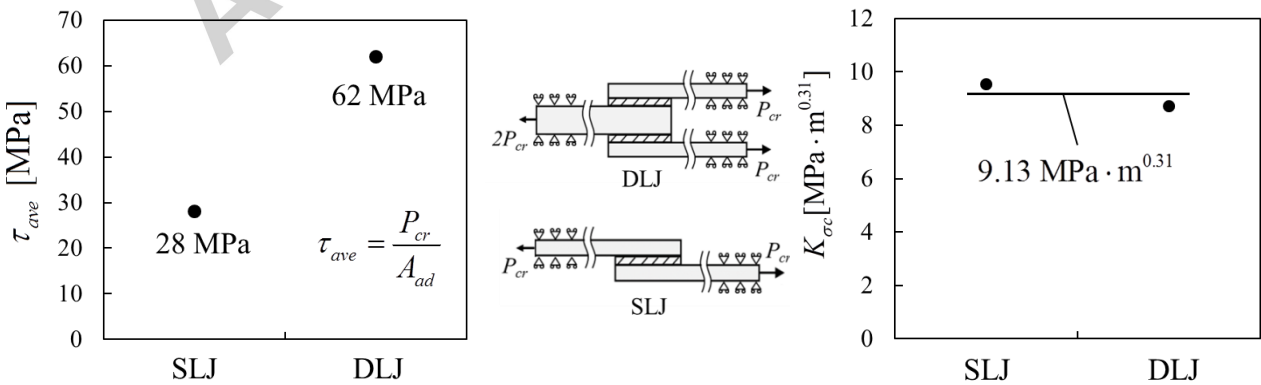


Fig.13 Unique relationship between  $K_{\sigma, \lambda_1}$  and  $\theta_C$ .

### 5. How to obtain the adhesive strength for double lap joint by using single lap joint

The experimental results show that the strength of double lap joint is about two times larger than the strength of single lap joint as shown in Fig.14 (a) [19]. However, the critical ISSF  $K_{\sigma_c}$  is the same for the double and single lap joints as shown in Fig.14 (b). In this section, therefore, the equivalent strength conditions for the SLJ on the DLJ in Fig. 15 will be considered in terms of the ISSF  $K_{\sigma, \lambda_1}$  by varying the adherend thickness  $t_1$ . In addition, since end tabs are often used by bonding at the ends of experimental specimens to reduce bend effect when loaded, the influence of the tab on  $K_{\sigma, \lambda_1}$  will be also considered. Here, the same material of the adherend is assumed for the tab.



(a) Average shear strengths of SLJ and DLJ

(b) The critical ISSF  $K_{\sigma_c}$  of SLJ and DLJ

Fig.14 Adhesive strength of single lap joint (SLJ) and double lap joint (DLJ) (Adherend: S45C, Adhesive: Epoxy)

B)

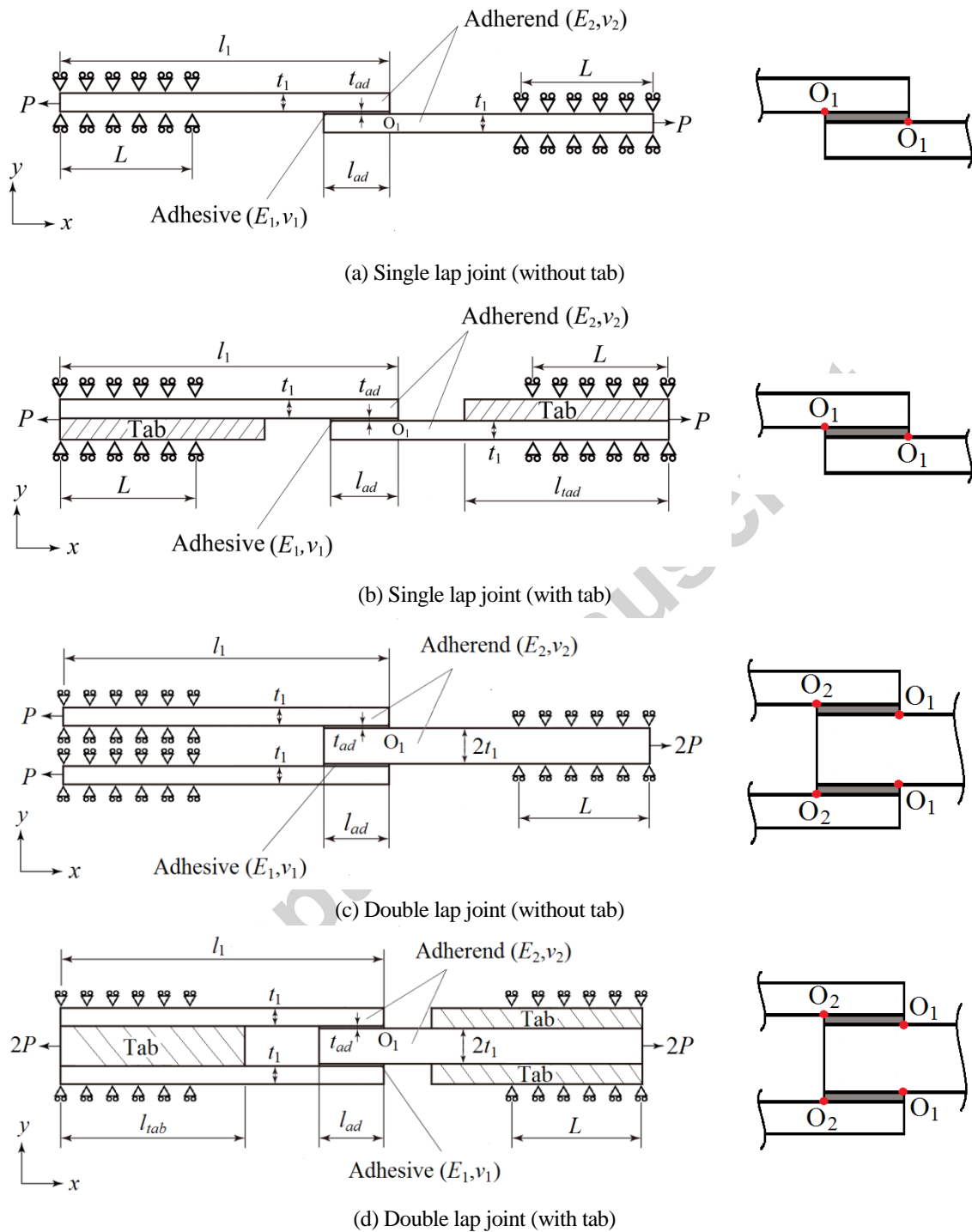


Fig. 15 Analysis models of lap joints

As shown in Fig.15 (a), (b) for the SLJ, both interface corners can be denoted as point “O<sub>1</sub>” because of the symmetry. However, as shown in Fig. 15 (c), (d) for the DLJ, since the ISSFs at the interface corners are different, they are denoted by corner “O<sub>1</sub>” and corner “O<sub>2</sub>”.

Fig. 16 shows the results of ISSF  $K_{\sigma,\lambda_1}$  at interface corners O<sub>1</sub> and O<sub>2</sub>. It is found that the  $K_{\sigma,\lambda_1}$  at corner O<sub>1</sub> is larger than that at corner O<sub>2</sub>. The  $K_{\sigma,\lambda_1}$  for the specimen with tab is nearly equal to the  $K_{\sigma,\lambda_1}$  for the specimen without tab. Therefore, the fracture may occur at corner O<sub>1</sub> during testing. For this reason, the equivalent conditions of strength for single lap joint and double lap joint will be considered by using the  $K_{\sigma,\lambda_1}$  at interface corner O<sub>1</sub>.

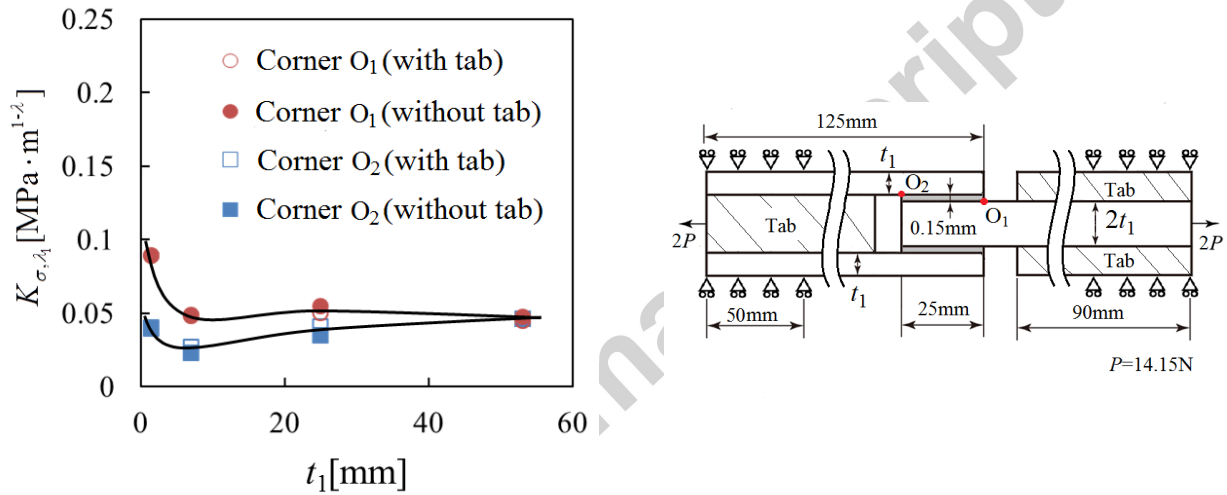


Fig. 16 ISSF  $K_{\sigma,\lambda_1}$  for double lap joint (see Fig. 15(c),(d))

Fig. 17 shows the ISSFs  $K_{\sigma,\lambda_1}$  at interface corner O<sub>1</sub> by varying the adherend thicknesses  $t_1$  for both single and double lap joints. Both ISSFs decrease with increasing adherend thickness  $t_1$ . When  $t_1 \geq 25$ mm, both ISSFs become constant independent of  $t_1$ . In JIS, the adherend thickness is prescribed as  $t_1 = 1.5$ mm. The  $K_{\sigma,\lambda_1}$  of the SLJ with  $t_1 = 7$ mm is nearly equal to the  $K_{\sigma,\lambda_1}$  of the DLJ with  $t_1 = 1.5$ mm (JIS). Similarly, the  $K_{\sigma,\lambda_1}$  of the SLJ is nearly equal to the  $K_{\sigma,\lambda_1}$  of the DLJ when  $t_1 \geq 25$ mm. By using those geometries the same adhesive strength can be obtained for SLJ and DLJ.

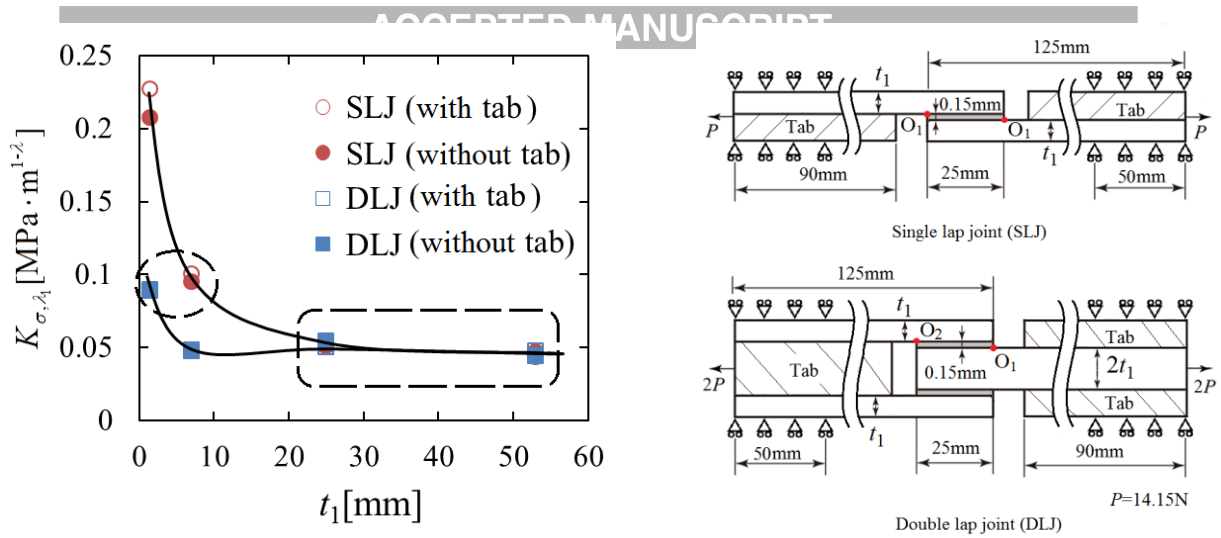
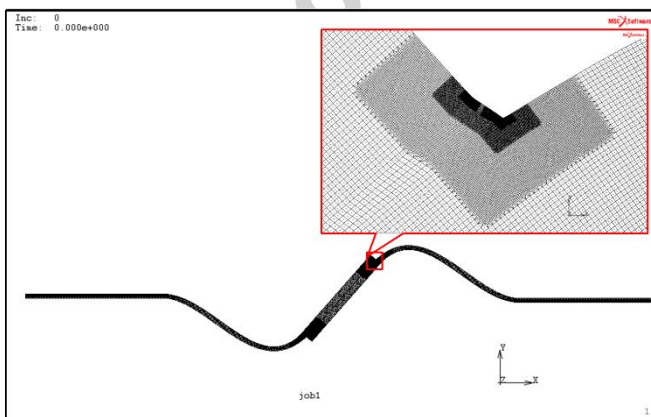
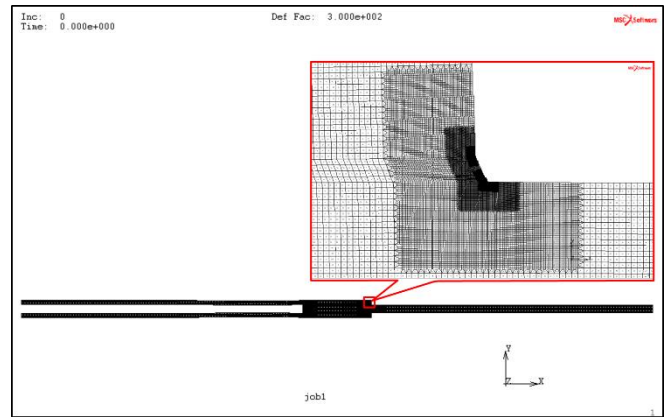


Fig. 17 Comparison of single lap joint (SLJ) and double lap joint (DLJ)

When adherend thickness  $t_1 \geq 25$ mm, the minimum ISSF  $K_{\sigma, \min}$  can be obtained as  $K_{\sigma, \min} = 0.0422 \text{ MPa} \cdot \text{m}^{1-\lambda_1}$ . Under this condition, the bend effect can be minimized. The reason why  $K_{\sigma, \min} \neq 0$  can be explained from slight local deformation observed at the interface end. The deformations of the lap joints in Fig. 17 without tab are shown in Fig. 18 where the deformation is magnified by 300 times. As can be seen from Fig. 18, when  $t_1=1.5$ mm, the bend deformation of the SLJ in Fig. 18 (a) is much large than the one of the DLJ in Fig. 18 (b). Instead, the bend deformation of SLJ with  $t_1=7$ mm in Fig. 18 (c) is nearly same as the bend deformation of DLJ with  $t_1=1.5$ mm in Fig. 18 (b). When  $t_1 \geq 25$ mm, all lap joint deformations are nearly the same, and there is only the local bend deformations for Figs. 18 (e)~(h).



(a) SLJ with  $t_1=1.5$ mm



(b) DLJ with  $t_1=1.5$ mm

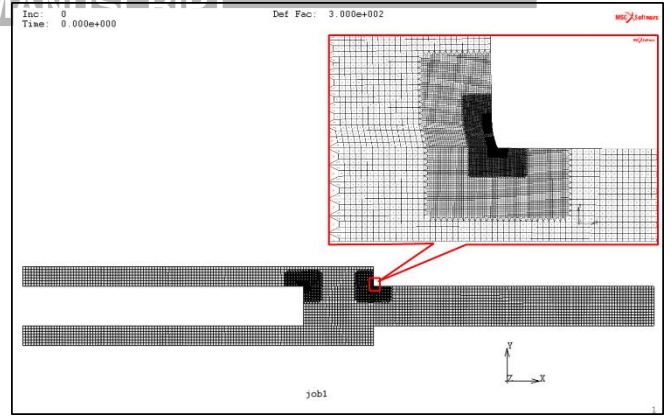
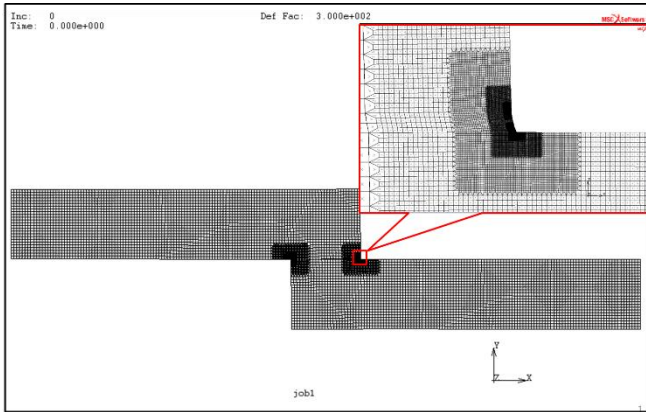
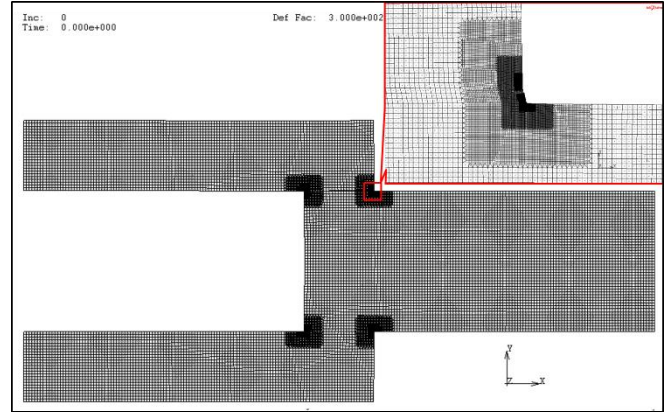
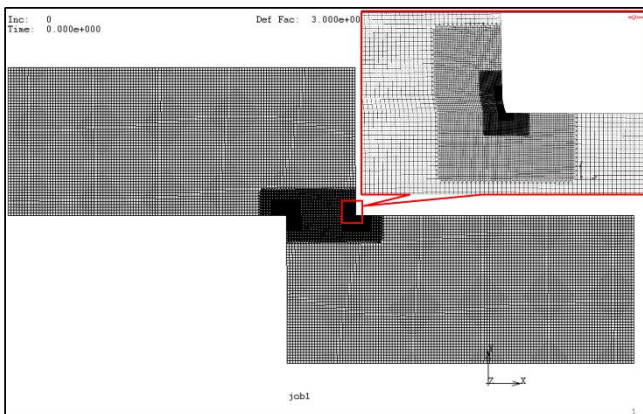
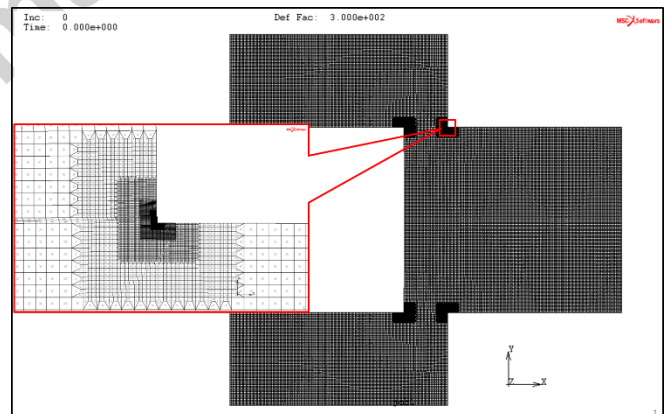
(c) SLJ with  $t_1=7\text{mm}$ (d) DLJ with  $t_1=7\text{mm}$ (e) SLJ with  $t_1=25\text{mm}$ (f) DLJ with  $t_1=25\text{mm}$ (g) SLJ with  $t_1=53\text{mm}$ (h) DLJ with  $t_1=53\text{mm}$ 

Fig. 18 Local deformations at the interface end in Fig.15 (the deformation is magnified by 300 times).

## 5. Conclusion

The lap joint testing was originally designed to investigate the adhesive strength under pure shear loading. However, actually pure shear testing is very difficult to be realized in the experiment because of the bend deformation during testing causing the peeling force appearing at

the adhesive region. To reduce the bend effect, this study focused on the ISSF at the interface end in order to minimize the ISSF for lap joints. The conclusions can be summarized in the following way.

- (1) The effect of specimen geometry was considered under the same adhesive geometry and the same magnitude of load. The ISSF  $K_{\sigma, \lambda_1}$  decreases with increasing adherend thickness  $t_1$  and the minimum  $K_{\sigma, \lambda_1}$  was obtained when the adherend thickness is large enough.
- (2) The single lap joint strength with the adherend thickness  $t_1 = 7\text{mm}$  is nearly equal to that of double lap joint with  $t_1 = 1.5\text{mm}$  prescribed in JIS. When the adherend thickness is large enough as  $t_1 \geq 25\text{mm}$ , the single and double lap joint strength is nearly equal the same.
- (3) The relationship between the ISSF  $K_{\sigma, \lambda_1}$  and deformation angle at the interface corner  $\theta_C$  was discussed. It was found that the ISSF  $K_{\sigma, \lambda_1}$  decreases with decreasing  $\theta_C$ , the minimum deformation angle can be obtained also when the adherend thickness  $t_1$  is large enough. The variation of ISSF can be uniquely controlled from the deformation angle at the interface corner. In other words, the bend effect in lap joints can be minimized when the adherend thickness is large enough.
- (4) The single lap joint strength with the adherend thickness  $t_1 = 7\text{mm}$  is nearly equal to that of double lap joint with  $t_1 = 1.5\text{mm}$  prescribed in JIS. When the adherend thickness is large enough as  $t_1 \geq 25\text{mm}$ , the single and double lap joint strength is nearly equal the same.

The previous study indicated that the ISSF is a promising method to predict and analyze the bonding-debonding behaviors [8-13]. The ISSF method shows good conformity with the experimental data as shown in Fig.1 (a), (b) and Fig. 14 (b). The final goal of this study is to establish a suitable pure shear testing method for adhesive strength by confirming the usefulness experimentally. The authors think that the experimental evidences to support the authors' conclusions can be obtained in future studies since the theoretical background has been indicated in this paper.

## Acknowledgement



## Appendix A: Singular index for lap joints

Table A.1 shows singular index for lap joints  $\lambda$  within a range of  $0 < \text{Re}(\lambda) < 1$ , where the underlined figure indicate the multiple root, the bold figure indicate the complex root, the standard style figure indicate the real root. The eigenequation (A.1) has real root, multiple real root or complex root depending on  $(\alpha, \beta)$  except for no root at  $(\alpha, \beta) = (-1, -0.5)$ . Two real roots appear in most of the material combinations.

$$4\sin^2(\pi\lambda)\left\{\sin^2\left(\frac{\pi\lambda}{2}\right)-\lambda^2\right\}\beta^2+4\lambda^2\sin^2(\pi\lambda)\alpha\beta+\left\{\sin^2\left(\frac{\pi\lambda}{2}\right)-\lambda^2\right\}\alpha^2-4\lambda^2\sin^2(\pi\lambda)\beta$$

$$-2\left\{\lambda^2\cos(2\pi\lambda)+\sin^2\left(\frac{\pi\lambda}{2}\right)\cos(\pi\lambda)+\frac{1}{2}\sin^2(\pi\lambda)\right\}\alpha+\sin^2\left(\frac{3\pi}{2}\lambda\right)-\lambda^2=0 \quad (\text{A.1})$$

**Table A.1** Singular index for lap joints  $\lambda$  ( $0 < \text{Re}(\lambda) < 1$ ). [ underlined figure indicate multiple root, **bold** figure indicate complex root, standard style figure indicate real root]

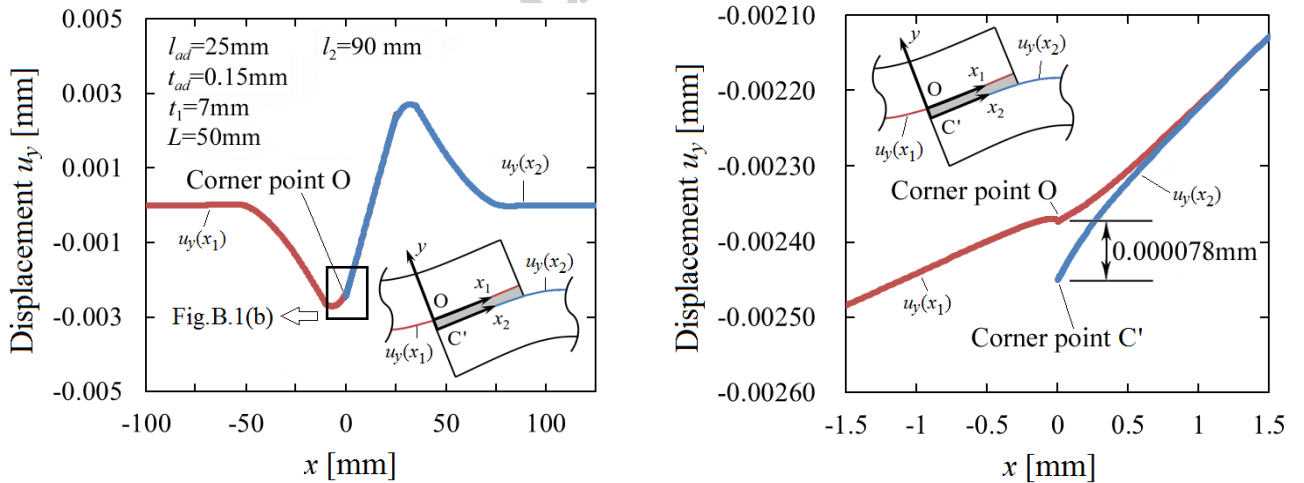
$\alpha$	$\beta=-0.5$	$\beta=-0.4$	$\beta=-0.3$	$\beta=-0.2$	$\beta=-0.1$	$\beta=0$	$\beta=0.1$	$\beta=0.2$	$\beta=0.3$	$\beta=0.4$	$\beta=0.5$
-1	Non	0.807313	0.720529	0.664609	0.624659	0.594612					
-0.9		0.800102	0.713270	0.657967	0.618663	0.589223					
-0.8		0.997323	0.998666	0.999111	0.999333	0.999467					
-0.7		0.794890	0.706604	0.651598	0.612819	0.583934					
-0.6		0.988598	0.994363	0.996246	0.997185	0.997748					
-0.5			0.700535	0.645489	0.607116	0.578738					
-0.4			0.986584	0.991068	0.993300	0.994638					
-0.3			0.695095	0.639636	0.601547	0.573629	0.552526				
-0.2			0.974790	0.983193	0.987375	0.989886	0.991563				
-0.1			0.690364	0.634041	0.596104	0.568599	0.548004				
0			0.958485	0.972217	0.979070	0.983201	0.985967				
0.1			0.686483	0.628716	0.590782	0.563645	0.543552				
0.2			0.937298	0.957761	0.968020	0.974246	0.978436				
0.3			0.683711	0.623685	0.585580	0.558760	0.539167				
0.4			0.911000	0.939524	0.953867	0.962655	0.968617				
0.5			0.682542	0.618989	0.580497	0.553941	0.534851	0.521047			
0.6			0.879395	0.917337	0.936302	0.948055	0.956113	0.961997			
0.7				0.614698	0.575537	0.549184	0.530605	0.517475			
0.8				0.891188	0.915116	0.930101	0.940505	0.948184			
0.9				0.610930	0.570707	0.544484	0.526433	0.514038			
1.0				0.861179	0.890238	0.908529	0.921385	0.930994			
1.1				0.607894	0.566022	0.539838	0.526433	0.514038			
1.2				0.827429	0.861739	0.883194	0.921385	0.930994			
1.3				0.606003	0.561511	0.535243	0.518343	0.507703	0.501847		
1.4				0.789888	0.829796	0.854095	0.871335	0.884461	0.894894		
1.5					0.557223	0.530697	0.514455	0.504921	0.500526		
1.6					0.794628	0.821357	0.840068	0.854257	0.865522		
1.7					0.553253	0.526195	0.510710	0.502536	0.500000		

	0.756400	0.785186	0.804636	0.819026	0.830167	
0.5	0.549802	0.521736	0.507168	0.500757	0.500737	
	0.715108	0.745794	0.765131	0.778569	0.788128	
0.6	0.547386	0.517317	0.503944	0.500000	0.503736	
	0.670322	0.703330	0.721601	0.732578	0.738354	
0.7		0.512937	0.501301	0.501267	0.511773	
		0.657821	0.673870	0.680168	0.678146	
0.8		0.508591	0.500000	0.508067	0.544319	<b>0.570579</b>
		0.609106	0.621093	0.617814	0.588069	$\pm 0.0645534i$
0.9		0.504280	0.504147	<b>0.532822</b>	<b>0.534652</b>	<b>0.537138</b>
		0.556769	0.558811	$\pm 0.0339893i$	$\pm 0.072084i$	$\pm 0.108448i$
1		0.500000	<b>0.500000</b>	<b>0.500000</b>	<b>0.500000</b>	<b>0.500000</b>
			$\pm 0.0319377i$	$\pm 0.0645318i$	$\pm 0.0985231i$	$\pm 0.134852i$
						$\pm 0.174850i$

## Appendix B: How to describe the bend deformation of the lap joints

In Appendix B, the bend deformation of the lap joints is presented. Assume that the total length of the specimen is 225mm, the adhesive length  $l_{ad}=25\text{mm}$ , adhesive thickness  $t_{ad}=0.15\text{mm}$ , fixed boundary length  $L=50\text{mm}$ , adherend length  $l_2=90\text{mm}$  and  $P=14.15\text{N}$ .

Fig. B.1 (a) shows displacements  $u_y(x_1)$ ,  $u_y(x_2)$  in the  $y$ - direction along the interfaces  $x_1$  and  $x_2$  when the adherend thickness  $t_1=7\text{mm}$ . As shown in Fig. B.1, displacement  $u_y(x_1)$  is skew-symmetric at the centre of the adhesive. Fig. B.1(b) shows the details at the interface end. As can be seen from Fig. B.1(b), small difference 0.000078mm can be seen at the interface end between  $u_y(x_1)$ ,  $u_y(x_2)$ .



(a) Displacement  $u_y(x_1)$  in the range  $x_1 = -100\sim 25$  and

Displacement  $u_y(x_2)$  in the range  $x_2 = 0\sim 150$

(b) Details at the interface ends in Fig.B.1(a)

Fig. B.1 Displacements  $u_y(x_1)$ ,  $u_y(x_2)$  in the  $y$ -direction along the two interfaces  $x_1$  and  $x_2$ .

Fig. B.2 defines several angles to describe the bend deformation. In order to obtain a deformation angle, two target points are considered. Here,  $l_\theta$  means the distance between the two target points. For the deformation angle  $\theta_{ol}$  at the interface corner O, the two target points O and A are used. For the deformation angle  $\theta_{or}$  at the interface corner O, the two target points O and B are used. For the deformation angle  $\theta_C$  at the interface corner C, two target points C and D are used. The deformation angles  $\theta_{ol}$ ,  $\theta_{or}$ ,  $\theta_C$  can be defined as follows.

$$\theta_{or} = \arctan\left(\frac{y_B - y_O}{x_B - x_O}\right), \theta_{ol} = \arctan\left(\frac{y_O - y_A}{x_O - x_A}\right), \theta_C = \arctan\left(\frac{y_C - y_D}{x_C - x_D}\right) \quad (\text{B.1})$$

Here,  $x_n$  and  $y_n$  ( $n = O, A, B, C, D$ ) are the coordinates of points O, A, B, C, D.

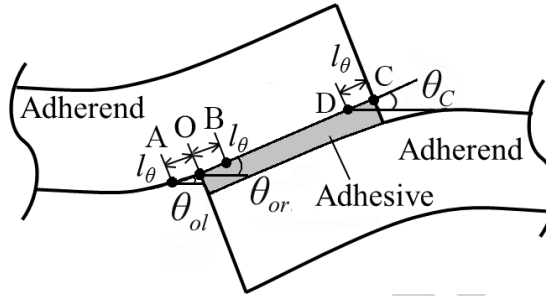


Fig.B.2 Deformation near the interface corner.

Fig. B.3(a) shows the results of deformation angles at corner O by varying distances  $l_\theta$  for  $t_1 = 7\text{mm}$ . It is found that both values of  $\theta_{ol}$  and  $\theta_{or}$  increase with increasing  $l_\theta$ , and the difference between  $\theta_{ol}$  and  $\theta_{or}$  increases with decreasing  $l_\theta$ . Therefore, it is not easy to obtain the maximum deformation angle at interface corner O. Fig.B.3(b) shows the results of deformation angle  $\theta_C$  by varying distances  $l_\theta$  for  $t_1 = 7\text{mm}$ . It is seen that the value of  $\theta_C$  initially increases and then decreases with increasing  $l_\theta$ . When the target point D approaches the interface end C beyond a certain limit distance, the increment of  $(x_C - x_D)$  becomes larger than the increment of  $(y_C - y_D)$  because the interface end C is on a free surface. This is the reason why  $\theta_C$  becomes smaller when  $l_\theta$  approaches zero as shown in Fig.B.3 (b). As an example shown in Table 3, the maximum  $\theta_C$  can be obtained when  $l_\theta = 1/3^3$  mm independent of element sizes.

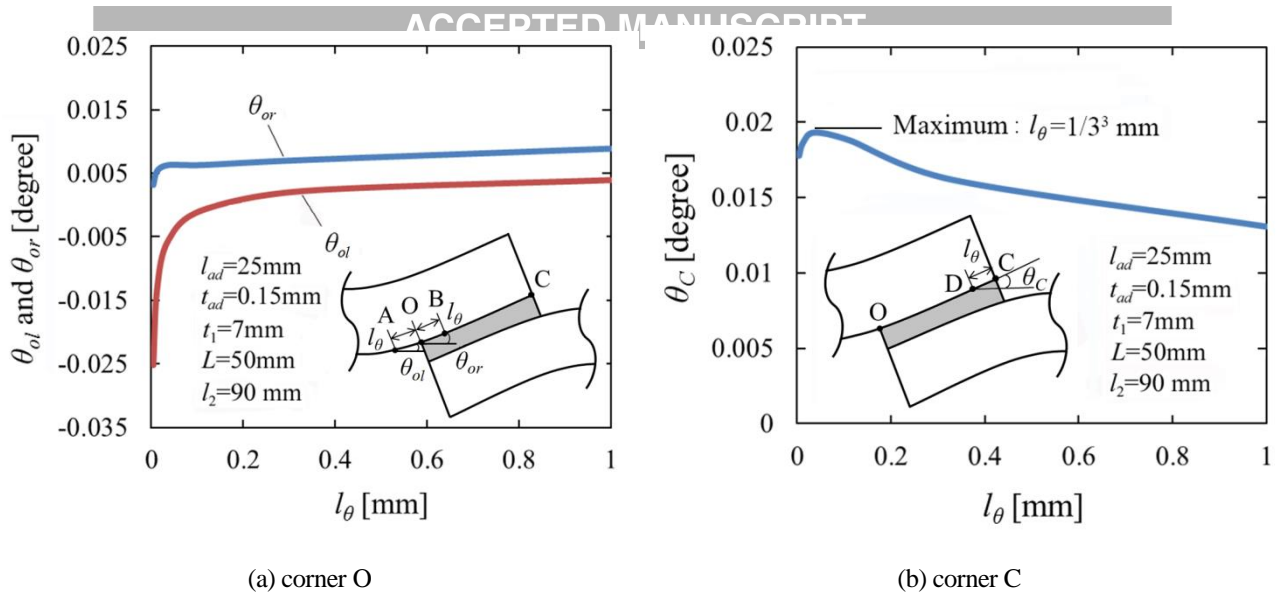


Fig.B.3 Deformation angle at interface corner edge.

Fig.B.4 shows the relationship between deformation angles  $\theta_{ol}$ ,  $\theta_{or}$  and  $\theta_C$ . It is found that the  $\theta_C - \theta_{ol}$  relation and  $\theta_C - \theta_{or}$  relation are almost linear, and the slope of the lines are nearly the same. Therefore, in this study, the deformation angle is considered by using the maximum  $\theta_C$  at corner C.

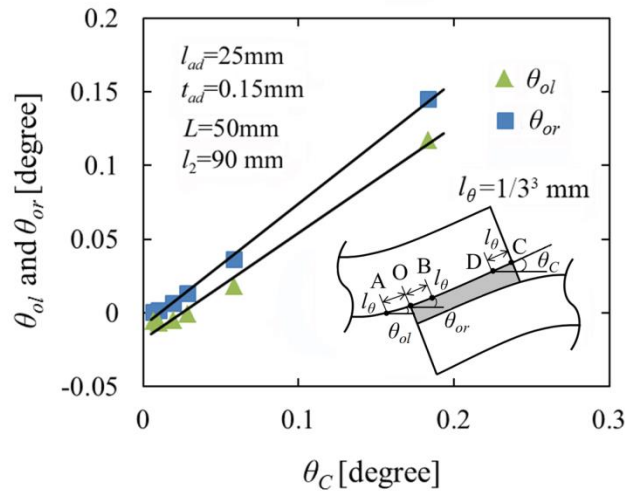


Fig. B. 4 Relationship between  $\theta_{ol}$ ,  $\theta_{or}$  and  $\theta_C$

### Appendix C: Effects of the bondline length and bondline thickness on the ISSF

In this study, under the fixed bondline dimensions  $l_{ad}=25\text{mm}$ ,  $t_{ad}=0.15\text{mm}$ , the most suitable testing conditions are investigated by changing  $L$  and  $t_1$ . The effects of bondline length  $l_{ad}$  and bondline thickness  $t_{ad}$  on ISSF were studied previously [9-13], the results in [9-13] are

presented as follows. In [9-13], the specimen used by Park was analyzed. The total length of the specimen is 225mm with adherend thickness  $t_1=7\text{mm}$  and  $d=10\text{mm}$ , the adherend lengths are in the range 77.5 – 97.5mm.

Figure C.1 (a) shows the effect of the bondline length  $l_{ad}$  under  $P/W=14.15\text{N/mm}$  [9-13]. It is seen that ISSF  $K_{\sigma,\lambda_1}$  decreases with increasing  $l_{ad}$  when  $l_{ad}\geq 15\text{mm}$ . Figure C.1 (b) shows the effect of the bondline thickness  $t_{ad}$  [9-13]. The solid line and dashed line denote the values of  $K_{\sigma,\lambda_1}$  for  $l_{ad}=25\text{mm}$  and  $30\text{mm}$ , respectively. It is found that  $K_{\sigma,\lambda_1}$  is insensitive to  $t_{ad}$ .

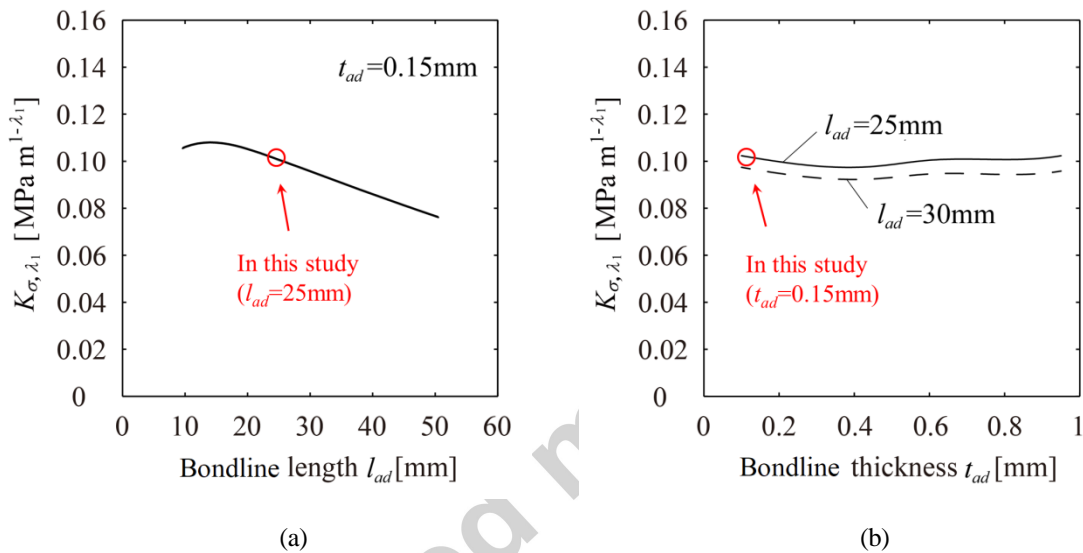


Fig. C.1 (a) Relationship between ISSF  $K_{\sigma,\lambda_1}$  and bondline length  $l_{ad}$ ; (b) Relationship between ISSF  $K_{\sigma,\lambda_1}$  and bondline thickness  $t_{ad}$  [9-13]

## References

- [1] Nozu, H., Kitada, T., Recent progress of adhesive and sealant in the automobile industry. Trans Soc Auto Eng Jpn, 1977, 31(10), 902-911 [in Japanese].
- [2] J Soc Mater Sci. Adhesion and materials. Shokabo, Tokyo; 1996 [in Japanese].
- [3] Lörinci, G., Matuschek, G., Fekete, J., Gebefügi, I., Kettrup, A., Investigation of thermal degradation of some adhesives used in the automobile industry by thermal analysis/mass spectrometry and GC-MS. Thermochim Acta 1995; 263: 73-86.
- [4] Barnes, T.A., Pashby, I.R., Joining techniques for aluminium spaceframes used in automobiles: Part II — adhesive bonding and mechanical fasteners. J Mater Process Tech 2000; 99(1-3): 72-79.

- [5] Xuemei, W., Vijay, G., Construction and characterization of chemically joined stainless steel/E-glass composite sections. *Mech Mater* 2005; 37(12): 1198-1209.
- [6] Jarry, E., Sheno, R.A., Performance of butt strap joints for marine applications. *Int J Adhes Adhes* 2006; 26(3): 162-176.
- [7] Encinas, N., Oakley, B.R., Belcher, M.A., Blohowiak, K.Y., Dillingham, R.G., Abenojar, J., Martínez, M.A., Surface modification of aircraft used composites for adhesive bonding. *Int J Adhes Adhes* 2014; 50:157-163.
- [8] Noda, N.A., Miyazaki, T., Li, R., Uchikoba T, Sano Y, Debonding strength evaluation in terms of the intensity of singular stress at the interface corner with and without fictitious crack. *Int J Adhes Adhes* 2015; 61: 46-64.
- [9] Miyazaki, T., Noda, N.A., Li, R., Uchikoba, T., Sano, Y., Debonding criterion for single lap joints from the intensity of singular stress field. *J Jpn Inst Electron Packag* 2013;16(2): 143-151 [in Japanese].
- [10] Miyazaki, T., Noda, N.A., Uchikoba, T., Li, R., Sano, Y., Proposal of a convenient and accurate method for evaluation of debonding strength. *Trans Soc Auto Eng Jpn* 2014; 45(5): 895-901 [in Japanese].
- [11] Miyazaki, T., Noda, N. A., Sano, Y., A precise and efficient analytical method to obtain two distinct intensities of singular stress fields for single lap joint. *J Jpn Inst Electron Packag* 2018; 21(2): 166-177 [in Japanese].
- [12] Miyazaki, T., Noda, N. A., Evaluation of debonding strength of single lap joint by the intensity of singular stress field. *J Phys Conf Ser* 2017; 842: 012078.
- [13] Noda, N. A., Li, R., Miyazaki, T., Takaki, R., Sano, Y., Convenient Adhesive Strength Evaluation Method in Terms of the Intensity of Singular Stress Field. *Int J Comput Methods* 2018; 15(1): 1850085-01 - 1850085-30.
- [14] Mintzas, A., Nowell, D., Validation of an  $H_{cr}$ -based fracture initiation criterion for adhesively bonded joints. *Eng Fract Mech* 2012; 80: 13-27.
- [15] Qian, Z., Akisanya, A.R., An experimental investigation of failure initiation in bonded joints.

- [16] Hattori, T., Iwasa, M., Fracture mechanics with bonding or contacting interfaces: II. A stress singularity parameters on a bonding or contact edge. *J Soc Mater Sci* 2000; 49(1): 123-129 [in Japanese].
- [17] Shibutani, T., Evaluation of crack initiation at interfacial edge on the basis of fracture mechanics concept and application to electronics devices (Tutorial series: foundations for reliability analysis). *J Jpn Inst Electron Packag* 2004; 7(7): 639-644 [in Japanese].
- [18] JIS K6850:1999, Adhesives-Determination of tensile lap-shear strength of rigid-to-rigid bonded assemblies [in Japanese].
- [19] Ikegami, K., Fujii, T., Kawagoe, H., Kyogoku, H., Motoie, K., Nohno, K., Sugibayashi, T., Yoshida, F., Benchmark tests on adhesive strengths in butt, single and double lap joints and double-cantilever beams. *Int J Adhes Adhes* 1996; 16(4):219-226.
- [20] Nakajima, A., Saito, M., Hino, H., Nishi, K., Suzuki, Y., Kodaka, A., Experimental study on fundamental strength characteristics of adhesive connection between steel members. *J Adhes Soc Jpn* 2011; 47(2): 53-59 [in Japanese].
- [21] Park, J.H., Choi, J.H., Kweon, J.H., Evaluating the strengths of thick aluminum -to-aluminum joints with different adhesive lengths and thicknesses. *Compos Struct* 2010; 92: 2226-2235.
- [22] Yuuki, R., *Mechanics of interface*. Baifuukann, Tokyo; 1993 [in Japanese].
- [23] Bogy, D.B., Edge-bonded dissimilar orthogonal elastic wedges under normal and shear loading. *Trans ASME J Appl Mech* 1968; 35: 460-466.
- [24] Bogy, D.B., Two edge-bonded elastic wedges of different materials and wedge angles under surface tractions. *Trans ASME J Appl Mech* 1971; 38: 377-386.
- [25] Dundurs, J., Discussion: "Edge-bonded dissimilar orthogonal elastic wedges under normal and shear loading". *Trans ASME J Appl Mech* 1969; 36: 650-652.
- [26] Zhang, Y., Noda, N.A., Wu, P.Z., Duan, M.L., A mesh-independent technique to evaluate stress singularities in adhesive joints. *Int J Adhes Adhes* 2015; 57:105–117.
- [27] Zhang, Y., Noda, N.A., Wu, P.Z., Duan, M.L., Corrigendum to A mesh-independent technique to

evaluate stress singularities in adhesive joints [Int J of Adhes Adhes, 2015; 57:105-117], Int J of Adhes Adhes, 2015; 60:130.

- [28] Adams, R., D., Peppiat, N., A., Stress analysis of adhesive-bonded lap joints, J Strain Anal Eng 1974; 9(3): 185-196.
- [29] Arai, M., Kobayashi, H., Adhesively bonded lap joints: Fracture mechanisms and strength evaluation. Trans Jpn Soc Mech Eng A 1998; 64(619): 74-79.
- [30] Campilho RDSG, Moura de MFSF, Domingues JJMS., Numerical prediction on the tensile residual strength of repaired CFRP under different geometric changes. Int J Adhes Adhes 2009; 29: 195-205.
- [31] Noda, N.A., Ren, F, Rei, Takaki, R., Wang, Z., Oda, K., Miyazaki, T., Sano, Y., A mesh-independent technique to evaluate stress singularities in adhesive joints. Int J Adhes Adhes 2018; 85: 234-250 (in press).